SYNTHESIS OF CAPA AND ITS ANALOGUES FOR ANALYSIS OF ANTI-

CANCER ACTIVITY, AND COMPUTATIONAL DOCKING OF CAPE,

CAPA AND ANALOGUES WITH THE DRS OF P38α

by

Mauricio A. Jemal, B.S.

A thesis submitted to the Graduate Council of
Texas State University in partial fulfillment
of the requirements for the degree of
Master of Science
with a Major in Biochemistry
August 2020

Committee Members:

Sean M. Kerwin, Chair

Liqin Du

Alexander Kornienko

FAIR USE AND AUTHOR'S PERMISSION STATEMENT

Fair Use

This work is protected by the Copyright Laws of the United States (Public Law 94-553, section 107). Consistent with fair use as defined in the Copyright Laws, brief quotations from this material are allowed with proper acknowledgement. Use of this material for financial gain without the author's express written permission is not allowed.

Duplication Permission

As the copyright holder of this work I, Mauricio A. Jemal, authorize duplication of this work, in whole or in part, for educational or scholarly purposes only.

ACKNOWLEDGEMENTS

TABLE OF CONTENTS

LIST OF TABLES

LIST OF FIGURES

Figure   **Page**

ABSTRACT

A Caffeic acid phenethyl amide (CAPA) is the amide derivative of caffeic acid phenethyl ester (CAPE), a bioactive extract from propolis. CAPE has been extensively studied and shown to be cytotoxic in many cancer cell lines. CAPE is also an inhibitor of angiogenesis and may decrease resistance to traditional chemotherapeutics. Although CAPE has been well characterized very little is known about the biological activity of CAPA. We synthesized a library of CAPA analogues to be used to treat various cancer cell lines to determine if the extensive cytotoxicity observed in CAPE is preserved. Previous studies have established that CAPE is a potent inhibitor of p38α through interactions with the D-recruitment site (DRS). We employed computational docking via AutoDock Vina to gain insight into the potential differentiation in modes of binding between CAPE and CAPA. This *in silico* work has revealed that CAPE preferentially binds to a previously unidentified hydrophobic pocket in the DRS whereas CAPE does not.

1. INTRODUCTION

1.1. CAPE as A Promising Anticancer Drug:
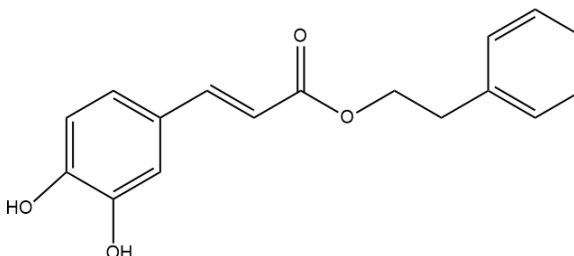
Propolis is the resinous material produced by most bee species that is used to strengthen and protect the hive. Since antiquity humans have used the propolis produced by worker bees for its natural antibacterial properties and to treat various ailments.[1] Caffeic acid phenethyl ester (CAPE) is a major component extracted from the propolis that has displayed significant biological activity. CAPE has been shown to reduce inflammation by reducing expression of NF-κB growth factors and acting as an antioxidant.[2, 3] CAPE is innocuous to normal cells and has demonstrated cytotoxicity in various cancer cell lines.[4, 5] Additionally, CAPE demonstrated cytoprotective effects against oxidative stress in human endothelial cells.[4] CAPE has been shown to induce apoptosis in leukemic HL-60 cells through activation of caspase-3, up-regulation of Bax and down-regulation of Bcl-2.[5] CAPE has been shown to inhibit growth of triple-negative breast cancer cells *in vitro* by inducing an S-phase cell cycle arrest.[3] Pre-clinical *in vivo* studies demonstrated a reduction in size of mouse xenographs by over 60% in 4 weeks.[3] It has been suggested that CAPE down-regulates expression of the mdr-1 gene which is responsible for resistance to chemotherapeutic agents pointing to a potential tandem treatment with traditional drugs.[3] CAPE has even been shown to increase radiosensitivity

1

by prolonging radiation-induced DNA Damage.[6] Cytotoxicity in multiple myeloma cells and neuroblastoma cells was observed as a result of increased oxidative stressed induced by CAPE.[7, 8] CAPE may also be effective as an antiangiogenic agent in breast and colon cancer cells which could halt the development of tumors by depriving them of oxygen and nutrients required for growth.[8, 9] Additionally, CAPE has been identified as a potential p38a inhibitor by acting on the D-recruitment site (DRS), which may play a role in its anti-cancer activity.[10] The wide range of targets combined with multiple mechanisms of action makes CAPE a favorable natural product for the development of anti- cancer drugs.

1.2. CAPA Has Improved Metabolic Stability
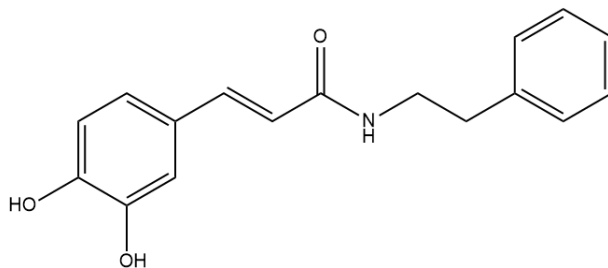
Despite the overwhelming therapeutic potential demonstrated by CAPE it is plagued by low bioavailability due to rapid metabolism. In rat plasma *in vivo* and *in vitro* CAPE was rapidly metabolized and pharmacokinetic studies indicate a rapid clearance from circulation.[11,12] This rapid metabolic breakdown can be attributed to CAPE having a high susceptibility to esterase enzymes.[11] Caffeic acid phenethyl amide (CAPA) is the amide derivative of CAPE in which the central ester is replaced with an amide. An amide bond is far less susceptible to esterase mediated hydrolysis so CAPA should have an increased permanence *in vivo* compared to CAPE.[13] It was established that CAPA was

significantly more stable in rat plasma. CAPA demonstrated a half-life of 10 hours at body temperature in rat plasma, a 77- fold increase from CAPE.[13] Studies conducted in male Sprague-Dawley rats established that CAPA was significantly more stable *in vivo* indicated by a 162.8 min increase in half-life compared to CAPE.[14] Although the amide bond in CAPA mitigates esterase hydrolysis the compound is still decomposed relatively rapidly, reducing its therapeutic potential. The catechol group on the molecule contains two hydroxy groups that are highly susceptible to phase II metabolism. For CAPA to serve as a viable drug it must persist for long enough to exert its effects. We hypothesize that if we change the constituents on the peripheral aromatic ring phase II metabolism can be mitigated thus further increasing the half-life of CAPA. To test this hypothesis CAPA and its analogues were subjected to in vitro metabolism in minipig microsomes. We monitored the disappearance of CAPA as it is converted to its glucuronide metabolites, elucidating its susceptibility to UGT-mediated phase II metabolism.

1.3. Cytotoxicity of CAPA in Cancer Cell Lines

The biological activity of CAPE has been established extensively whereas the therapeutic capability of CAPA is not as well understood. It has been established that CAPA acts as an antioxidant retaining the cytoprotective properties in endothelial HUVEC cells observed in CAPE.[15] We synthesized CAPA and a library of analogues intended to increase the half-life of CAPA in turn improving the bioavailability of the compound. Our aim is to establish the therapeutic potential of CAPA in treating neuroblastoma and multiple myeloma. We hope to achieve this by exposing the analogues to the cell lines and determine the extent of cytotoxicity. We have coordinated

with collaborators to test the compounds for cytotoxicity in neuroblastoma cell lines, multiple myeloma cell lines and lung cancer cell lines. Because of the wide range of cancer cell lines that CAPE is active in, we have many potential targets to experiment with using CAPA.

1.4. Computational Docking with the p38α DRS

Mitogen-activated protein kinases (MAPKs) are highly conserved protein kinases whose signal cascades control several complex cellular functions such as cell growth, differentiation, proliferation and cell death.[16] They are so ubiquitous and essential to cell function that they comprise 2% of the mammalian genome.[17] Due to their instrumental role in cell signaling and survivability many MAPKs are known to play a vital role in cancer cell survival.[18] MAP kinases are activated by upstream proteins known which belong to the MEK family.[16] Upon phosphorylation by MEKs, MAP kinases become highly activated and initiate a phosphorylation cascade. [16] Although they bear many similarities in structure and function MAPKs are distributed into several different groups. Those groups include extracellular signal-regulated kinases 1 and 2 (ERK1 & ERK2), ERK5, Jun amino terminal kinases 1-3 (JNK1, JNK2 & JNK3) and p38 (α, β, γ & δ).[19] The p38 module is consisted of several proteins knows as MAPKKKs, MAPKKs and the four known p38 isoforms.[20] Activation of the p38 pathway is essential to normal immune function through; the production of inflammatory cytokines, activation of enzymes that control connective tissue remodeling and by playing a regulatory role in the proliferation and differentiation of immune cells.[21]

The specificity of all the MAPK groups is mediated, in part, by interactions with

scaffold protein which facilitate localization and the formation of complexes.[16] Specificity is also achieved using docking domains where high affinity interactions with the substrate can occur. [16] The specificity of these docking domains makes them a favorable target drug development. One of the regions of the protein responsible for its specificity known as the D-recruitment site has been shown to be a promising drug binding site in JNK, ERK and p38α.[22,23,10]

CAPE was shown to act as a potential allosteric inhibitor of p38α through interaction with the DRS.[10] This was discovered by using a type of N-alkynylimidazole as a small molecule probe. Using click chemistry, the probe formed an adduct with p38α through covalent interaction with Cys119. The adduction of this probe is selectively inhibited by ligands that bind in the DRS of p38α.[10] By incubating p38α with a library of ligands, a number of small molecules were identified as novel p38α inhibitors. CAPE was among these novel inhibitors, however, it was observed that CAPA did not demonstrate the same inhibitory effects as CAPE.[10] To understand why in this instance the activity of CAPE was not observed with CAPA we conducted a computational docking study on various p38α crystal structures and our library of CAPA analogues. We simulated interactions between the analogues and the DRS and then compared them to the simulated CAPE docking. Our aim was to elucidate the interactions that CAPE engages in to determine if we observe a comparable interaction with CAPA. In addition to determining the interactions undergone by CAPA and CAPE, a library of CAPA analogues were also computationally docked with the DRS of p38α. We aimed to explore how replacing the catechol group of CAPA with various substituted phenyl rings might affect the mode of binding to p38α.

2. MATERIALS AND METHODS

2.1. Reagents and equipment:

The following reagents were obtained commercially and used as received: 3-methoxy-4-hydroxybenzaldehyde was purchased from Chem-Impex (Wood Dale, IL). Piperonal, 3,4-dihydroxybenzaldehyde and potassium carbonate were acquired from Sigma-Aldrich (St. Louis, MO). tert-Butyldimethylsilyl chloride (TBDMSCl), tetrabutylammonium fluoride (TBAF), dichloromethane (DCM), phenethyl alcohol, chloroacetyl chloride and cesium carbonate were purchased from Acros Organics (Geel, Belgium). Sodium sulfate and sodium chloride was obtained from Fisher Scientific (Waltham, MA). Triphenylphosphine was purchased from Alfa Aesar (Haverhill, MA). The hydrochloric acid (HCl), hexanes, and ethyl acetate (EtOAc) were acquired from Merk Millipore (Burlington, MA). Silica powder was obtained from SiliCycle (Quebec, Canada). Tetrahydrofuran (THF) was obtained from Sigma-Aldrich (St. Louis, MO) and distilled from sodium/benzophenone immediately before use. Nuclear magnetic resonance spectra were obtained using a 400 MHz Bruker (Billerica, MA). Infrared spectroscopy data was collected using an FT/IR – 4600 manufactured by JASCO Inc. (Tokyo, Japan).

2.2. Synthesis of CAPA and Analogues:

Preparation of Wittig Reagent:
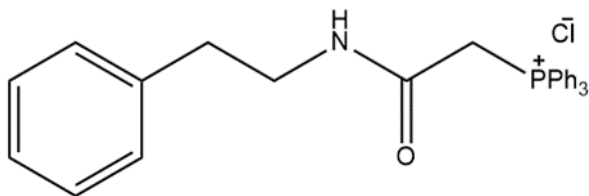
Phenethylcarbamoylmethyl-triphenylphosphonium chloride (1): A solution of triphenylphosphine (10.1 mmol, 1.5 eq) was prepared in freshly distilled THF (40 mL). To the solution was added 2-chloro-N-phenethylacetamide (2.0g, 15.2 mmol) and the mixture was stirred in an oil bath at 110 °C for 18 h. The resulting reaction mixture was then diluted with DCM and the solid was filtered yielding a fine white powder (2.23 g, 52% yield). ^{1}H NMR matches literature.[15]

General Procedure for Silyl Protection:
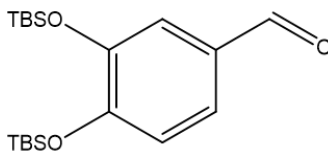
3,4-Bis-((ter-butyldimethyl-silyl)oxy)benzaldehyde (2): A solution of 3,4-dihydroxybenzaldehyde (1.77 g, 13.6 mmol) was prepared in anhydrous DCM. To the solution, 6 equivalents of imidazole were added and subsequently, 2.4 equivalents of tert-butyldimethyl-silyl chloride (32.64 mmol) were added dropwise. The mixture was stirred for 4 h and the reaction was quenched with a volume of ice-cold DI water equivalent to the volume of the reaction mixture. The aqueous layer was extracted with DCM 3 times and then the resulting organic phase was washed with 30 mL of 1 N HCl. The organic

phase was then washed with brine and dried over Na_2SO_4. The solution was concentrated

under reduced pressure and purified on silica gel using flash chromatography with 10%

EtOAc in hexanes yielding 3.9 g of a white solid (78% yield). ^{1}H NMR (CDCl_3, 400

MHz) δ 9.80 (s, 1H), 7.37 (d, J = 2.0 Hz, 1H), 7.35 (d, J = 1.3 Hz, 1H), 6.93 (d, J = 8.5

Hz, 1H), 0.99 (s, 9H), 0.98 (s, 9H), 0.23 (s, 6H), 0.22 (s, 6H). ^{1}H NMR matches

literature.[29]
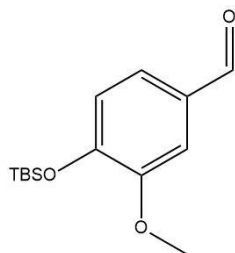
4-{[Dimethyl(2-methyl-2-propanyl)silyl]oxy}-3-methoxybenzaldehyde (2b):

Following the standard procedure above but starting with 4-hydroxy-3-

methoxybenzaldehyde (3.0 g, 19.7 mmol), Column chromatography (20%

EtOAc/Hexane) and recrystallization in EtOAc and hexanes afforded 4.55 g of white

solid (87% yield). ^{1}H NMR (CDCl_3, 400 MHz) 9.84 (s, 1H), 7.39 (d, J = 1.9 Hz, 1H),

7.36 (d, J = 3.3 Hz, 1H), 6.96 (d, J = 7.9 Hz, 1H), 3.87 (s, 3H), 1.00 (s, 9H), 0.19 (s, 6H).

^{1}H NMR matches literature.[25]

General Procedure for Witting Reaction:
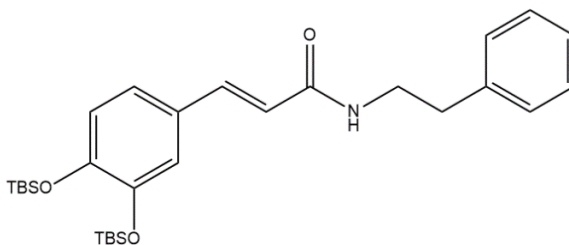
(*E*)-3-(3,4-bis((tert-butyldimethylsilyl)oxy)phenyl)-*N*-phenethylacrylamide (3a): The di-TBSO protected benzaldehyde 2 (500 mg, 1.3 mmol) was dissolved in 4.5 mL of 1,4-dioxane in an oven dried pear bottom flask. A separate oven dried flask was charged with Cs$_2$CO$_3$ (2.6 eq, 2.3 mmol) and dried under vacuum with a heat gun. The same flask was charged with the Phenethylcarbamoylmethyl-triphenylphosphonium chloride (1.2 eq, 1.1 mmol) and 4.5 mL of DCM was added. The solution of di-TBSO benzaldehyde 2 was added slowly via a gas tight syringe. The reaction mixture was heated under reflux for 18 h in a 60 °C oil bath. The resulting mixture was filtered and concentrated under reduced pressure. The crude product was purified by column chromatography (25% EtOAc/Hexane), affording 120 mg (40% yield) as a yellow oil. ^{1}H NMR (CDCl$_3$, 400 MHz) δ 7.51 (d, J = 15.5 Hz, 1H), 7.34-7.23 (m, 5H), 7.0 (s, 2H), 6.8 (d, J = 8.2 Hz, 1H), 6.16 (d, J = 15.5 Hz, 1H), 5.7 (s, 1H), 3.7-3.6 (q, J = 6.6 Hz, 2H), 2.9 (t, J = 6.9 Hz, 2H), 1.0 (s, 9H), 0.98 (s, 9H), 0.2 (s, 6H), 0.19 (s, 6H). ^{1}H NMR matches literature.[15]
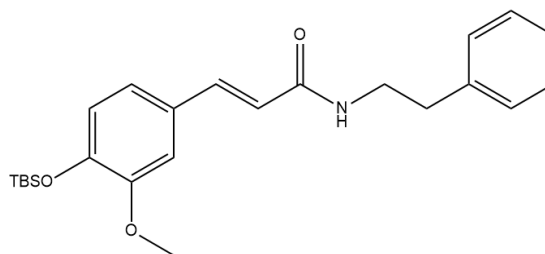
(2*E*)-3-((4- tert-butyldimethylsilyl)oxy)-3-methoxyphenyl)-*N*-(2-phenylethyl)acrylamide (3b): Following the standard procedure above but starting with TBSO protected vanillin (2b) (1.0 g, 3.8 mmol), Column chromatography (25% EtOAc/Hexane) and recrystallization in EtOAc and hexanes afforded 248 mg of a colorless oil (16% yield). ^{1}H NMR (CDCl$_3$, 400 MHz) δ 7.55 (d, J = 15.6 Hz, 1H), 7.32 (d, J = 7.5 Hz, 2H), 7.22 (t, J = 4.0 Hz, 3H), 6.99 (d, J = 8.2 Hz, 2H), 6.82 (d, J = 7.9 Hz, 1H), 6.21 (d, J = 15.5 Hz, 1H), 5.66 (s, 1H), 3.80 (s, 3H), 3.67-3.63 (q, J = 6.6 Hz, 2H), 2.88 (t, J = 6.7 Hz, 2H), 0.99 (s, 9H), 0.16 (s, 6H). ^{13}C NMR (CDCl$_3$, 400 MHz) δ 166.16, 151.12, 146.94, 141.03, 138.98, 128.82, 128.68, 126.53, 121.50, 121.07, 118.56, 111.04, 55.46, 40.76, 35.73, 25.66, 18.47, -4.59.
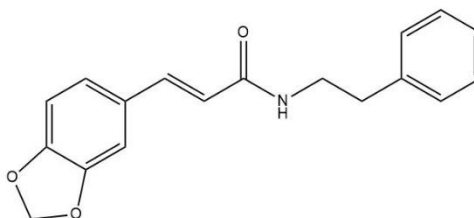
(2*E*)-3-(1,3-Benzodioxol-5-yl)-*N*-(2-phenylethyl)acrylamide (3c): Following the standard procedure above but starting with benzo[d][1,3]dioxole-5-carbaldehyde (1.0 g, 6.7 mmol), Column chromatography (25% EtOAc/Hexane) and recrystallization in EtOAc and hexanes afforded 417 mg of a powdered white solid (11% yield). ^{1}H NMR (CDCl$_3$, 400 MHz) δ 7.53 (d, J = 15.5 Hz, 1H), 7.32 (d, J = 7.5 Hz, 2H), 7.23 (dd, J = 3.9

Hz, 3H), 6.98 (s, 2H), 6.79 (d, J = 4.2 Hz, 1H), 6.14 (d, J = 15.5 Hz, 1H), 5.98 (s, 2H),

5.55 (s, 1H), 2.89 (t, J = 6.9 Hz, 2H). ^{1}H NMR matches literature.[26]
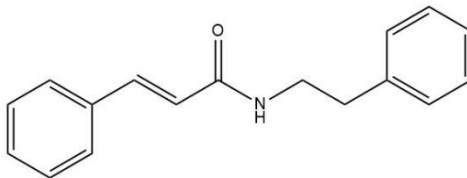
(2*E*)-3-Phenyl-*N*-(2-phenylethyl)-2-propenamide (3d): Following the standard

procedure above but starting with benzaldehyde (1.0 g, 9.4 mmol), Column

chromatography (10% EtOAc/Hexane) and recrystallization in EtOAc and hexanes

afforded 674 mg of a fibrous white solid (28% yield). ^{1}H NMR (CDCl$_3$, 400 MHz) δ 7.61

(d, J = 15.6 Hz, 1H), 7.48 (m, 2H), 7.34 (m, 5H), 7.24 (m, 3H), 6.31 (d, J = 15.6 Hz, 1H),

4.12 (q, J = 7.2 Hz, 2H), 3.67 (q, J = 6.5 Hz, 2H), 2.89 (t, J = 6.9 Hz, 2H). ^{1}H NMR

matches literature.[27]

General procedure for the deprotection Reaction:
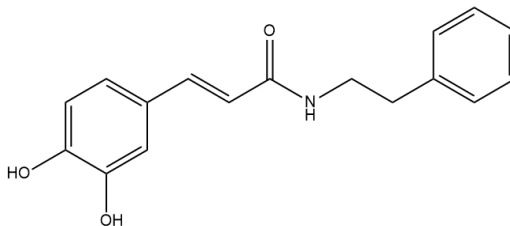
(2*E*)-3-(3,4-Dihydroxyphenyl)-*N*-(2-phenylethyl)acrylamide (4a): The di-TBSO

protected CAPA (120mg, 0.23 mmol) was dissolved in distilled anhydrous THF (1.1 mL)

(**4**) in an oven dried flask. Using a gas tight syringe TBAF (0.5 mL, 1M in THF) was

added dropwise and the mixture was stirred for 5 min at 0 C. The resulting mixture was

then concentrated on a rotary evaporator and subjected to chromatography on a silica gel

column (60% EtOAc/Hexane) yielding 2.7 mg of a colorless oil (5% yield). ^{1}H NMR (CDCl$_3$, 400 MHz) δ 7.54 (2, J = 15.6 Hz, 1H), 7.31 (d, J = 7.6 Hz, 2H), 7.23 (m, 3H), 7.11 (d, J = 2.1 Hz, 1H), 6.96 (d, J = 3.4 Hz, 1H), 6.86 (d, J = 8.2 Hz, 1H), 6.14 (d, J = 15.5 Hz, 1H), 5.68 (s, 1H), 3.65 (q, J = 6.6 Hz, 2H), 2.88 (t, J = 6.9 Hz, 2H). ^{1}H NMR matches literature.[15]
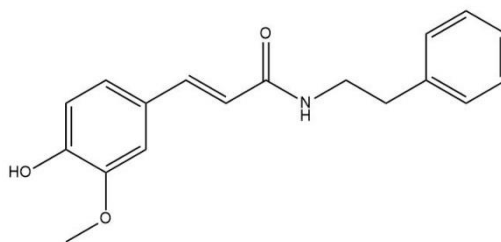
(**2E**)-**3-(4-Hydroxy-3-methoxyphenyl)-*N*-(2-phenylethyl)acrylamide (4b):** Following the standard procedure above but starting with (2E)-3-((4- tert-butyldimethylsilyl)oxy)-3-methoxyphenyl)-N-(2-phenylethyl)acrylamide (4b) (1.0 g, 6.7 mmol), Column chromatography (35% ETOAc/Hexane) and recrystallization in EtOAc and hexanes afforded 32.8 mg of a yellow oil (46% yield). ^{1}H NMR (CDCl$_3$, 400 MHz) δ 7.49 (d, J = 15.6 Hz, 1H), 7.35 (s, 1H), 7.26 (m, 4H), 7.16 (m, 2H), 7.05 (d, J = 3.4 Hz, 1H), 6.85 (d, J = 8.2 Hz, 1H), 6.53 (d, J = 15.7 Hz, 1H), 3.86 (s, 1H), 3.57 (q, J = 3.6 Hz, 2H), 2.99 (s, 1H). ^{1}H NMR matches literature.[28]

2.3. Synthesis of Fluorinated CAPE:
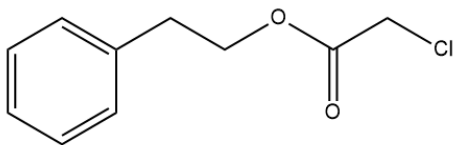
2-Phenylethyl chloroacetate (5): Phenethyl alcohol (21 mmol) was dissolved in 40 mL of distilled DCM in an oven dried flask and dried K_2CO_3 (22 mmol, 1.17 eq) was added swiftly. Using a gastight syringe chloroacetylchloride (22 mmol) was added dropwise and the resulting reaction mixture was stirred under argon for 18 h at 45 C. The resulting mixture was diluted with DCM and transferred to a separatory funnel and washed with water and brine. The resulting solution was dried with Na_2SO_4, filtered, then concentrated under reduced pressure yielding 3.8 g of colorless oil (91% yield). ^{1}H NMR (CDCl$_3$, 400 MHz) δ 7.33 (t, J = 3.6 Hz, 2H) 7.25 (m, 3H), 4.42 (t, J = 7.0 Hz, 2H), 4.04 (s, 2H), 2.99 (t, J = 7.1 Hz, 2H). ^{1}H NMR matches literature.[24]
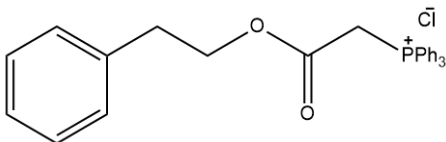
Phenethyloxycarbonylmethyl-triphenyl-phosphonium chloride (6): In a oven dried round bottom flask, 2-phenylethyl chloroacetate (7) (2.5 mmol) was dissolved in a 15 mL of distilled THF. In a separate oven dried pear bottom flask triphenyl phosphine (3.8 mmol, 1.5 eq) was dissolved in 5 mL of THF. The triphenyl phosphine solution was added dropwise to the reaction vessel with a gastight syringe. The solution was stirred for 24 h and a white precipitate formed. The solution was diluted with DCM and filtered, the filtrate was then washed with DCM, yielding 385 mg of a white powder (33% yield). [1]H

NMR (CDCl₃, 400 MHz) δ 7.63 (m, 20H), 6.93 (t, J = 4.0 Hz, 2H), 5.50 (d, J = 13.9 Hz, 2H), 4.07 (t, J = 7.0 Hz, 2H). ¹H NMR matches literature.[24]
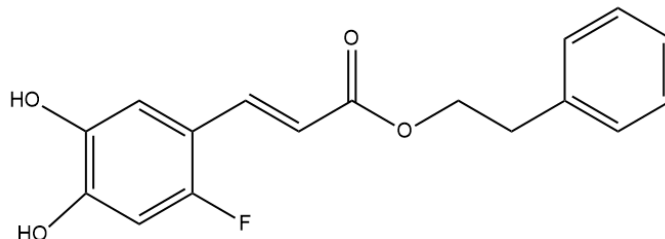
2-Phenylethyl (2*E*)-3-(2-fluoro-4,5-dihydroxyphenyl)acrylate (7): The 2-fluoro-4,5-dihydroxybenzaldehyde was dissolved in 5 mL of 1,4-dioxane in an oven dried round bottom flask. Dried K₂CO₃ (0.96 mmol, 1.5 eq) was added swiftly to the same flask. In a dry pear bottom flask, the phosphonium chloride was dissolved in 5 mL of DCM. From the pear bottom flask, the phosphonium chloride (0.89 mmol, 1.4 eq) was added slowly to the reaction vessel using a gastight syringe. The reaction mixture was refluxed at 60 °C and stirred for 24 hours in a hot oil bath. Upon completion the reaction mixture was filtered, washed with DCM, and subsequently concentrated under reduced pressure. Column chromatography (55% EtOAc/Hexane) and recrystallization afforded 6.4 mg (3.3% yield) of white crystals. ¹H NMR (acetone-D6, 400 MHz) δ 8.91 (s, 1H), 8.23 (s, 1H), 7.66 (d, J = 16.1 Hz, 1H), 7.30 (d, J = 4.5 Hz, 3H), 7.25 (m, 4H), 7.14 (d, J = 7.3 Hz, 1H), 6.67 (d, J = 11.6 Hz, 1H), 6.31 (d, J = 16.1 Hz, 1H), 4.36 (t, J = 6.7 Hz, 2H), 3.73 (q, J = 6.6, 2H), 2.99 (t, J = 7.0, 2H). ¹H NMR matches literature.[4]

2.4. Computational Docking of CAPE and CAPA to p38α:

All protein structures were acquired from the Protein Data Bank (PDB) was established at Brookhaven National Laboratories (Upton, New York). All PDBQT file preparation and docking simulations were conducted using AutoDock tools and AutoDock vina, programs developed by the Scripps Center for Mass Spectrometry and Metabolomics (San Diego, California). The molecular structures of the CAPA and CAPE analogues (ligands) were drawn and exported as a Simplified Molecular Input Line Entry Specification (SMILES) string using ChemDraw an application developed by PerkinElmer (Waltham, Massachusetts). All docking output files were visualized using Chimera a program developed by the Resources for Biocomputing Visualization, and Informatics (University of California, San Francisco). Additionally, interactions were inferred by atom proximity using Chimera.

General procedure for ligand preparation:

The bond line structure of the CAPE, CAPA, and its analogues were constructed in ChemDraw and copied as a SMILES string. The SMILES string was them imported into Chimera and converted to a three-dimensional structure. Chimera was then used to add AM1-BCC charges to nonstandard residues and the structure was minimized and saved as a Mol2 file. The ligand was then imported to AutoDock tools to be prepared for docking. The rotatable bonds were assigned using the torsion tree function and the ligand was saved as a PDBQT file.

General procedure for p38α preparation:

The crystal structure of p38α imported into AutoDock tools after it was acquired from The Protein database as a PDB file. Using AutoDock tools the solvating water molecules were removed from the crystal structure. Then using the same program, the polar hydrogens were added to the structure and the molecule was selected for docking and saved as a PDBQT file.

General procedure for docking the ligands with p38α:

Using AutoDock tools, the grid box was configured to a size and position that completely encompasses the DRS site surrounding the cys-119 on the p38α crystal structure. The coordinates and dimensions used for the grid box with a spacing of 1.0 angstroms were as follows:

$$center\_x = 33.33$$

$$center\_y = 44.973$$

$$center\_z = 20.025$$

$$size\_x = 18.0$$

$$size\_y = 20.0$$

$$size\_z = 28.0$$

The energy range used for this docking study was 4 with an exhaustiveness of 32. Upon completion of the protein and ligand preparation and the box configuration the conditions were saved as a txt document. AutoDock vina was then used through the command prompt and docking was carried out. Nine Poses for the ligand were generated along with

16

scores for each pose and the poses were visualized with the p38α crystal structure using

Chimera.

3. RESULTS AND DISCUSSION

3.1. Docking CAPE and CAPA to p38α DRS

To ensure that the conclusions drawn from the docking results are general, four different crystal structures of p38α were used for docking in AutoDock Vina. This is essential because the conditions used for crystallization and any ligands bound during the crystallization process can significantly alter the final protein structure, particularly of the docking recognition site (DRS). The PDB files used for this study were the highest resolution structure 1A9U and, the next highest resolution structure 1LEW. Additionally, the ligands were docked with the PDB files 5OUJ and 2OZA.

CAPE Docked with p38α:

Figure 1: Graphical representation of highest affinity CAPE pose docked with the crystal structure of p38α (PDB 1A9U). Hydrogen bonds are colored green and nearby residues with H-bond donors and acceptors are colored cyan. All residues within 4 Å are shown as stick figures in light gray.

Table 1: Nine poses generated from docking CAPE with the p38α crystal structure (PDB 1A9U) in AutoDock Vina. Affinity is measured by binding energy in kcal/mol. The variability of the poses compared to the highest scored pose is reported as root-mean-square deviation (Å).

mode	affinity (kcal/mol)	dist from best mode rmsd l.b.	rmsd u.b.
1	-7.2	0.000	0.000
2	-7.0	2.256	9.671
3	-7.0	2.448	10.029
4	-6.9	6.269	7.955
5	-6.8	6.327	7.985
6	-6.7	5.120	7.781
7	-6.6	5.547	8.310
8	-6.6	6.568	7.919
9	-6.6	4.247	8.605

The Docking simulations of CAPE with the DRS of p38α yielded high affinity poses which indicates an energetically favorable binding energy (Table 1). The upper bound RMSD values are high which indicates that there was high variability in the poses when compared to the highest scored pose. These findings corroborate the experimental data collected by Li. et al. who suggested that CAPE is capable of binding to the DRS and inhibiting adduct formation with their probe and p38α.

Structural analysis of the CAPE ligand docked with p38α conducted in UCSF Chimera (Fig. 1) elucidated several interactions that could explain why the binding to p38α is favorable. The hydrophobic phenyl group is clearly inserted into the hydrophobic pocked created by the Ile83, Val 84 and Leu164 residues (appendix Fig. 13) The Asn 82 residue was predicted to form a hydrogen bond with the carbonyl oxygen in the CAPE ligand, additionally the Tyr 132 and the hydroxyl group in the para position of the catechol form a hydrogen bond. The hydroxyl group in the meta position of the catechol group on CAPE is in close proximity to Arg 136 which may allow for a hydrogen bond to form despite it not being detected by chimera.
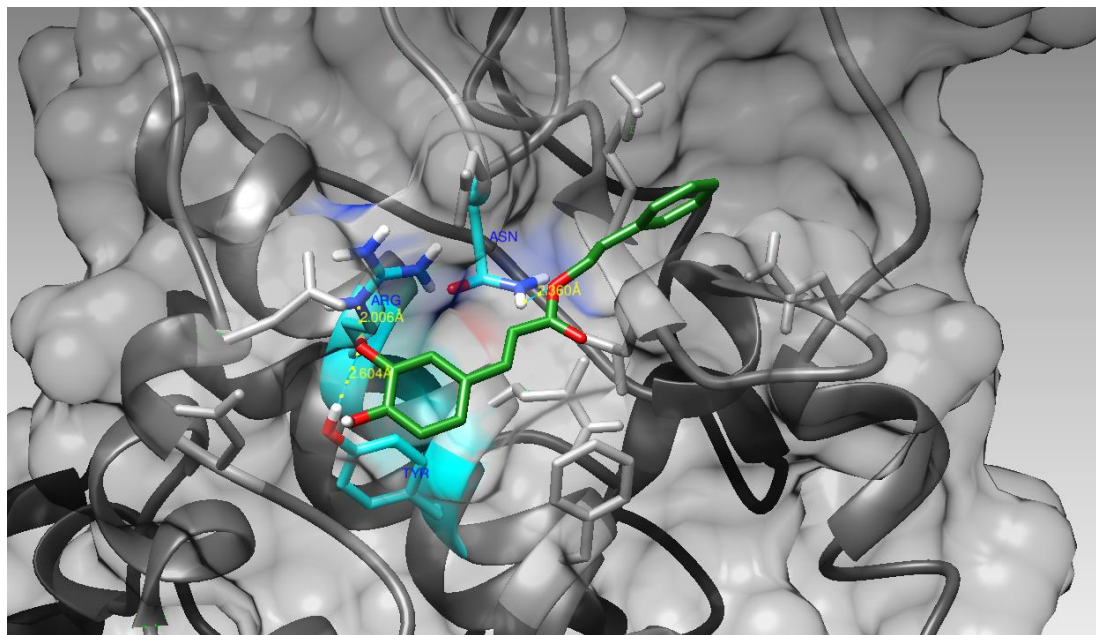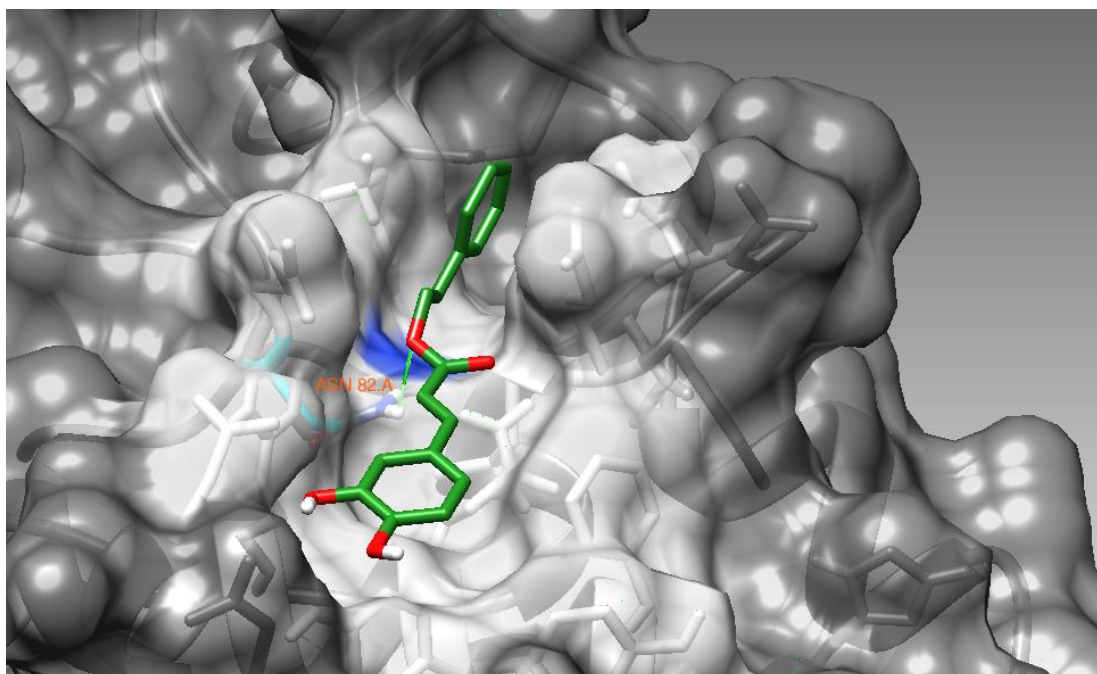
Figure 2: Graphical representation of highest affinity CAPE pose docked with the crystal structure of p38α (PDB 5UOJ). Hydrogen bonds are colored green and nearby residues with H-bond donors and acceptors are colored cyan. All residues within 4 Å are shown as stick figures in light gray.

Table 2: Nine poses generated from docking CAPE with the p38α crystal structure (PDB 5UOJ) in AutoDock Vina. Affinity is measured by binding energy in kcal/mol. The variability of the poses compared to the highest scored pose is reported as root-mean-square deviation (Å).

mode	affinity (kcal/mol)	dist from best mode rmsd l.b.	rmsd u.b.
1	-7.4	0.000	0.000
2	-7.1	1.254	1.974
3	-7.0	2.913	9.937
4	-7.0	2.496	3.784
5	-6.8	4.000	5.991
6	-6.8	6.252	8.199
7	-6.7	5.183	8.015
8	-6.7	2.172	9.681
9	-6.6	5.149	8.399

The affinity data obtained by docking CAPA with the 5UOJ crystal structure indicates favorable interactions between the ligand and protein. Additionally, the top two poses are similar in orientation as indicated by a low RMSD value for pose two.

Structural analysis performed in chimera shows that the ester oxygen in CAPA is

engaged in a hydrogen bond with the Asn 82 residue that was bound to the carbonyl

oxygen in the 1A9U crystal structure. Importantly the phenyl end of the CAPA ligand is

inserted into the deep hydrophobic pocket also engaged in the 1A9U. The repetition of

this bond taken with the favorable binding energy suggest that binding to in this pocket

contributes to affinity between the ligand and the protein significantly.

Figure 3: Graphical representation of highest affinity CAPE pose docked with the crystal
structure of p38α (PDB 1LEW). Hydrogen bonds are colored green and nearby residues
with H-bond donors and acceptors are colored cyan. All residues within 4 Å are shown as
stick figures in light gray.

Table 3: Nine poses generated from docking CAPE with the p38α crystal structure (PDB 1LEW) in AutoDock Vina. Affinity is measured by binding energy in kcal/mol. The variability of the poses compared to the highest scored pose is reported as root-mean-square deviation (Å).

```
mode |   affinity  | dist from best mode
     |  (kcal/mol) | rmsd l.b.|  rmsd u.b.
-----+-------------+----------+---------
  1         -5.5       0.000       0.000
  2         -5.5       3.519       5.223
  3         -5.4       2.702       5.993
  4         -5.4       3.550       6.728
  5         -5.3       3.642       6.243
  6         -5.3       2.546       6.572
  7         -5.3       4.135       7.015
  8         -5.3       3.721       7.572
  9         -5.3       1.908       5.611
```

When using the 1LEW structure of p38α the binding scores are somewhat less favorable that the scores predicted when using the 1A9U and 5UOJ structures (table 3). This may be explained by the hydrophobic pocket that was occupied by the phenyl group in the 1A9U and 5UOJ structure (Fig. 1&2) being less accessible in this crystal conformation. Despite the lower binding scores the upper bound RMSD values are much lower and remain fairly consistent in all poses. These results indicate a stable bond is formed despite the binding energy being higher.

Structural analysis of the CAPE ligand bound to 1LEW revealed that the carbonyl of the central ester was engaged in a hydrogen bond with ASN 82. This interaction was also predicted by the docking of CAPE with the 1A9U and 5UOJ structure (Fig. 1&2). The presence of this bond in both structures suggests that it plays a major role in stabilizing the interaction of the CAPE ligand with p38α. The second interaction predicted by structural analysis is between the same carbonyl oxygen in CAPE and the hydrogen bond donor ARG 136. This differs from the interaction predicted by docking to 1A9U in which the hydroxyl group in the catechol that was hydrogen bonding with TYR 132 and was within binding distance to ARG 136 (fig. 1). This discrepancy could arise as

a result of the position of the ligand on the p38α structure. Because the hydrophobic

pocket was not engaged by the phenyl group on the opposite flank of the ligand, the

catechol group was not able to occupy the correct position necessary to engage in a

hydrogen bond with TYR 133. In addition to the favorable entropic effects of engaging

the hydrophobic pocket, the positioning of the ligand while in the pocket allows it to

engage in more hydrogen bonds. That dual action may help explain why engaging in the

hydrophobic pocket is so vital to a strong protein-ligand interaction. Alternatively, this

could be explained by the slightly different position of the α-helices containing the
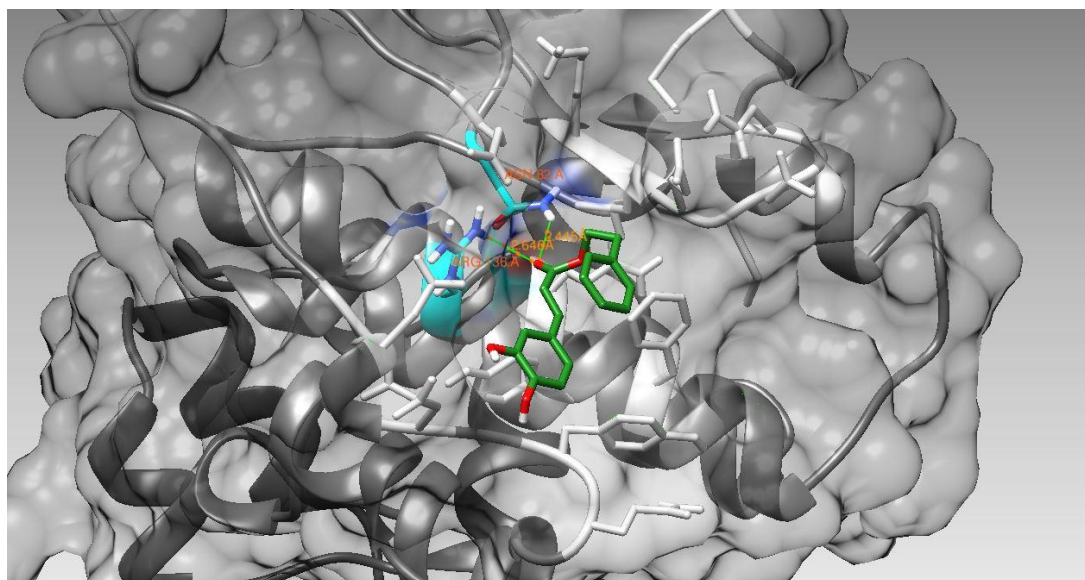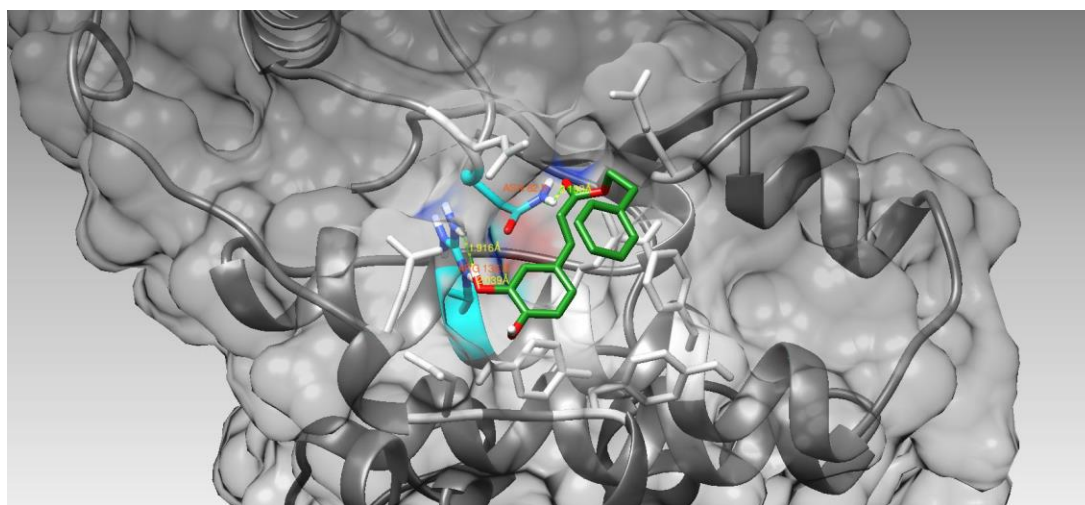
residues in each crystal structure.

Figure 4: Graphical representation of highest affinity CAPE pose docked with the crystal structure of p38α (PDB 2OZA). Hydrogen bonds are colored green and nearby residues with H-bond donors and acceptors are colored cyan. All residues within 4 Å are shown as stick figures in light gray.

Table 4: Nine poses generated from docking CAPE with the p38α crystal structure (PDB 2OZA) in AutoDock Vina. Affinity is measured by binding energy in kcal/mol. The variability of the poses compared to the highest scored pose is reported as root-mean-square deviation (Å).

mode	affinity (kcal/mol)	dist from best mode rmsd l.b.	dist from best mode rmsd u.b.
1	-5.8	0.000	0.000
2	-5.6	1.564	5.487
3	-5.6	2.414	5.747
4	-5.5	2.690	3.649
5	-5.4	2.101	5.074
6	-5.4	2.285	5.805
7	-5.4	2.317	5.770
8	-5.3	3.403	5.051
9	-5.3	3.165	5.671

The affinity scores generated form the simulated docking of CAPE with 2OZA are strikingly similar to the scores generated from docking CAPE with 1LEW (table 3). The binding energy (table 4) was lower that the scores generated from docking CAPE with 1A9U and 5UOJ (table 1,2), indicating a less favorable interaction. Additionally, the RMSD values are lower than those observed with 1A9U and more consistent, indicating low variability between the poses.

Inspection of the graphical representation of binding and structural analysis reveals that CAPE binds to the 2OZA structure in a similar manor to the binding observed with 1LEW. There is a predicted hydrogen bond between the ester carbonyl of CAPE and ASN 82 which has been predicted in all the docking studies we conducted. Despite the suboptimal position of the ligand there is still a hydrogen bond formed between the catechol hydroxyl group and ARG 136. However, as was observed in docking with 1LEW the Tyr 132 residue was not engaged in a hydrogen bond with the catechol of the ligand. This graphical representation of the protein surface reveals that the entrance to the hydrophobic containing the Ile116 and Leu122 residues is obstructed by

two glutamate. The ligand is not tucked into the hydrophobic pocket as was observed in 1A9U and 5UOJ binding (fig.1&2). The less favorable binding energy observed with an obstructed hydrophobic pocket supports the hypothesis that insertion of the phenyl group of CAPE to the hydrophobic pocket in the DRS is required for tight binding.

CAPA Docked with p38α:

Figure 5: Graphical representation of highest affinity CAPA pose docked with the crystal structure of p38α (PDB 1A9U). Hydrogen bonds are colored blue and nearby residues with H-bond donors and acceptors are colored cyan. All residues within 4 Å are shown as stick figures in light gray.

Table 5: Nine poses generated from docking CAPA with the p38α crystal structure (PDB 1A9U) in AutoDock Vina. Affinity is measured by binding energy in kcal/mol. The variability of the poses compared to the highest scored pose is reported as root-mean-square deviation (Å).

mode	affinity (kcal/mol)	dist from best mode rmsd l.b.	rmsd u.b.
1	-7.1	0.000	0.000
2	-6.9	1.023	2.052
3	-6.9	6.316	8.006
4	-6.7	8.513	10.750
5	-6.7	1.344	1.798
6	-6.6	6.797	9.626
7	-6.6	2.676	8.740
8	-6.4	3.093	8.736
9	-6.3	2.559	3.328

Docking simulations between CAPA and the p38α crystal structure 1A9U

produced a relatively low binding energy which is indicative of favorable interactions.

The RMSD values generated are generally high; however, poses 2, 5, and 9 are within the

desirable range (0-3.5 Å).

Analysis of the graphical representation of the docking output reveals that CAPA

is capable of engaging in a hydrogen bond with the Tyr 132 reside that was also observed

to interact with CAPE (Fig. 1). The pose with the best binding affinity appears to not be

interacting with the same pocket that was observed when CAPE was docked with the

same PDB file. Upon analysis of the less favorable poses for CAPA it is revealed that

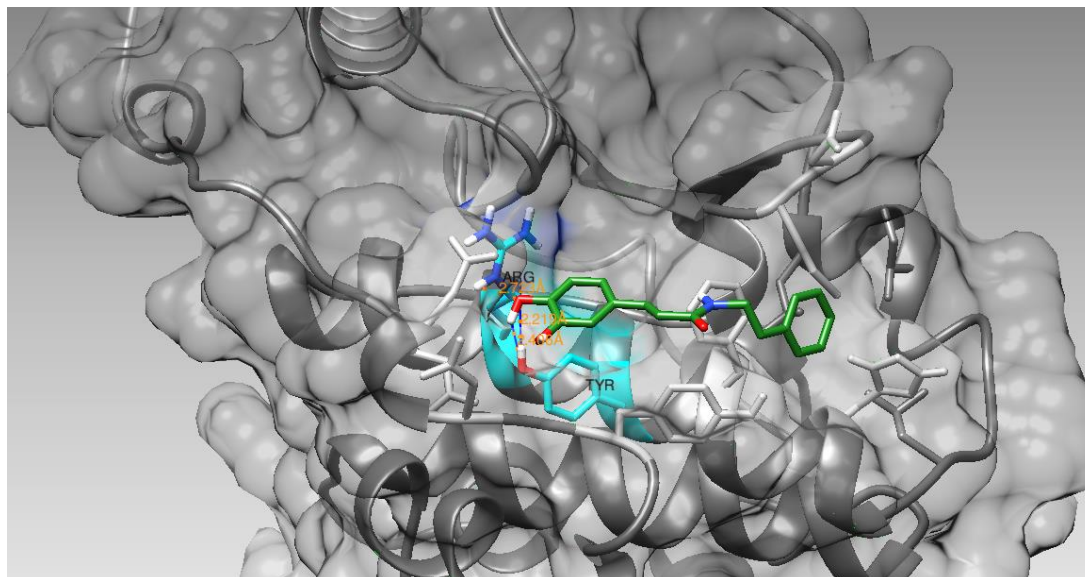some of the poses do engage this pocket (Appendix Fig. X).
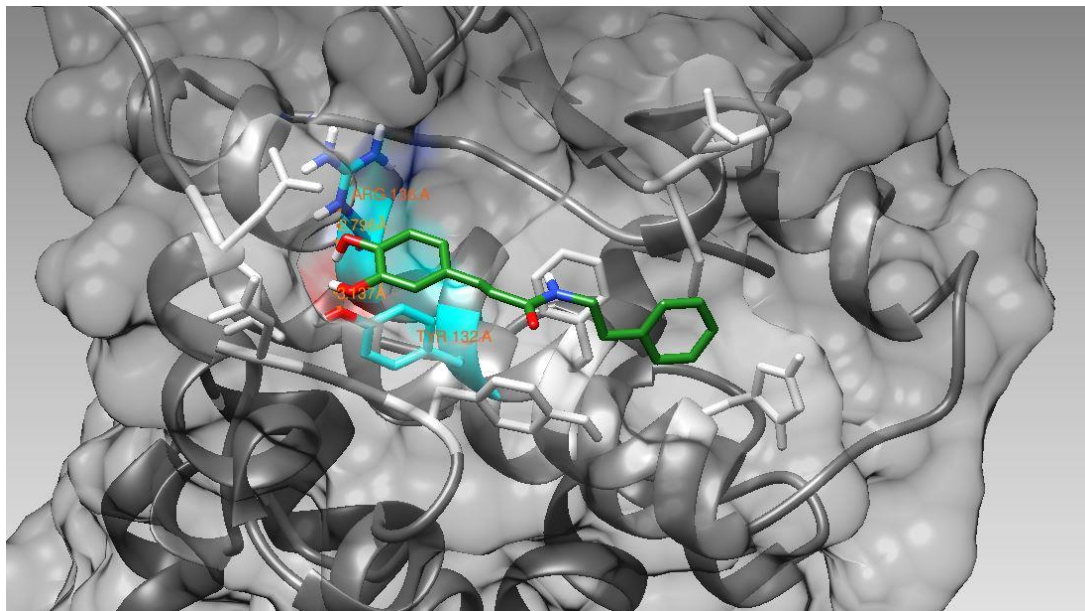
Figure 6: Graphical representation of highest affinity CAPA pose docked with the crystal
structure of p38α (PDB 1LEW). Hydrogen bonds are colored green and nearby residues
with H-bond donors and acceptors are colored cyan. All residues within 4 Å are shown as
stick figures in light gray.

Table 6: Nine poses generated from docking CAPA with the p38α crystal structure (PDB 1LEW) in AutoDock Vina. Affinity is measured by binding energy in kcal/mol. The variability of the poses compared to the highest scored pose is reported as root-mean-square deviation (Å).

```
mode |   affinity  | dist from best mode
     |  (kcal/mol) | rmsd l.b.| rmsd u.b.
-----+-------------+----------+----------
  1        -6.9        0.000       0.000
  2        -6.8        0.064       1.063
  3        -6.8        0.627       1.482
  4        -6.7        5.201       7.815
  5        -6.7        5.550       7.381
  6        -6.4        2.792       8.718
  7        -6.4        2.547       8.903
  8        -6.4        5.164       8.261
  9        -6.4        2.805       8.929
```

The affinity data obtained from docking simulation between CAPA and the 1LEW crystal structure of p38α is fairly similar the data obtained from docking CAPA with 1A9U. The binding energy is only slightly higher indicating a similar strength of binding. The RMSD values for the three most favorable poses are low indicating that the lowest energy pose (Fig. 5) is indeed the most likely conformation of the ligand while bound to p38α.

The graphical representation reveals that despite being in a similar orientation as it was when bound to 1A9U, there are no hydrogen bonds predicted by Chimera. This could be explained by the different position of the helix containing the Tyr 132 in this structure. Because the binding energies are similar, it may be inferred that that bond is not the primary contribution to the stability of CAPA while bound to p38α. However, due to the close proximity of the Arg 136 and Tyr 132 it is possible a hydrogen bond could occur in solution. The recurrence of the orientation observed previously (Fig.4) and the consistent RMSD scores suggest that the orientation of the CAPA molecule is in its

lowest energy state and it differs substantially in orientation from the CAPE ligand.
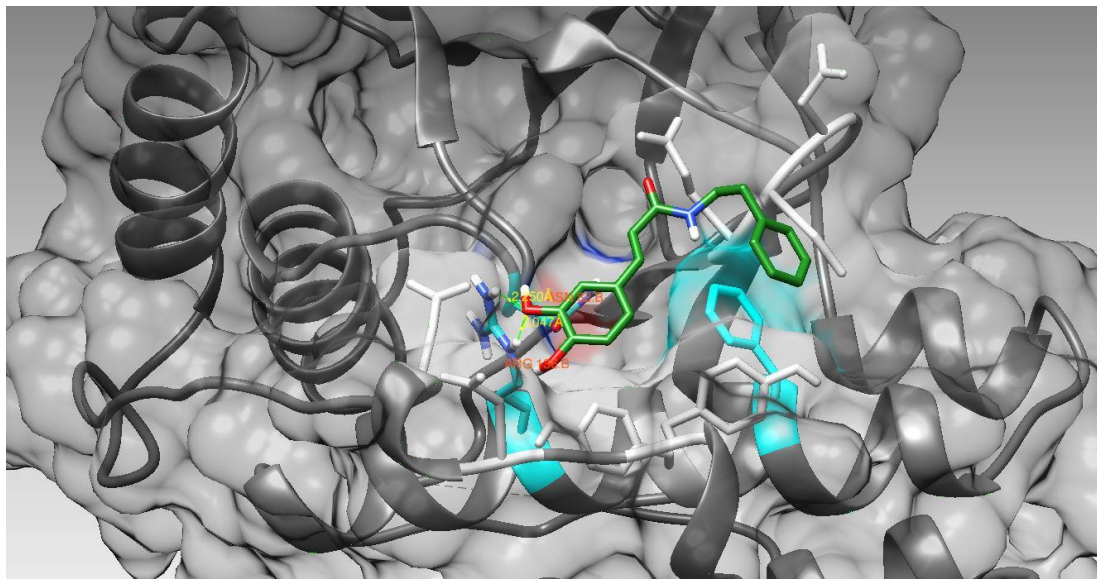
Figure 7: Graphical representation of highest affinity CAPA pose docked with the crystal structure of p38α (PDB 2OZA). Hydrogen bonds are colored green and nearby residues with H-bond donors and acceptors are colored cyan. All residues within 4 Å are shown as stick figures in light gray.

Table 7: Nine poses generated from docking CAPA with the p38α crystal structure (PDB 2OZA) in AutoDock Vina. Affinity is measured by binding energy in kcal/mol. The variability of the poses compared to the highest scored pose is reported as root-mean-square deviation (Å).

mode	affinity (kcal/mol)	dist from best mode rmsd l.b.	rmsd u.b.
1	-6.5	0.000	0.000
2	-6.2	2.239	2.940
3	-6.2	2.281	3.135
4	-6.1	4.525	7.861
5	-5.9	4.031	8.250
6	-5.9	4.054	8.293
7	-5.9	2.529	3.554
8	-5.8	3.796	6.829
9	-5.8	5.180	8.814

The computational data obtained by docking CAPA with 2OZA (Fig.6) indicates a similar affinity to shown with the previous two crystal structures (Fig. 4&5). In addition, the RMSD values for several poses are low which indicates the top pose is representative of most poses. In this simulation the hydroxyl in the catechol group is

hydrogen bonding with the Arg 136 residue. The hydrophobic phenyl end of the ligand is oriented over a minor hydrophobic pocket potentially coordinating with the Phe 129 residue.

Difference in p38α Inhibition by CAPE and CAPA:

In all three of the graphical representations of CAPA bound to different p38α crystal structures the polar catechol group is positioned near the Arg 136 and the Tyr 132 residues and can even engage in hydrogen bonds with either residue (Fig. 5,6&7). The hydrophobic phenyl group on the opposite end of the ligand is oriented towards the right side of the DRS in all major poses. These results are very different from the most favorable poses observed with CAPE. The lowest binding energy occurred when the hydrophobic end of cape was allowed to insert into the deep hydrophobic pocket created by the Ile83, Val 84 and Leu164 residues on the left side of the DRS. These *in silico* results indicate that the mode of binding for CAPA and CAPE may be different in solution.

It has been previously established through the use of a DRS probe that CAPE binds strongly to the DRS of p38α. Conversely, CAPA did not demonstrate the ability to inhibit adduct formation. In our *in silico* study we established that CAPA and CAPE may have distinct modes of docking. CAPE is at its lowest energy state when positioned in a deep hydrophobic pocket whereas CAPA only bound there in a high energy, unfavorable state. Taken with the previous experimental work our results may suggest that binding to this hydrophobic pocket could be necessary to inhibit p38α adduct formation. This process may occur through allosteric effects causing a conformational change in the DRS upon binding of the observed hydrophobic pocket by the ligand.

3.2. Docking of CAPA analogues:

In addition to the comparative study between CAPE and CAPA a number of CAPA analogues were also docked with p38α *in silico.* Our aim was to gain insight into how changing the constituents of the aromatic ring on the carbonyl side of CAPA may affect the mode of binding and therefore the biological activity of the compounds. The CAPA analogues were docked to p38α crystal structures 19AU (Fig. 9 & 11) and 1LEW (appendix Fig. 18 & 19) using AutoDock Vina and subsequent structural analysis was performed using UCSF Chimera. These PDB files were used because they represent the two highest resolution crystal structures available. Additionally, the previously described hydrophobic pocket is unobstructed which allows us to determine if the analogues binds in an orientation similar to CAPE or CAPA.
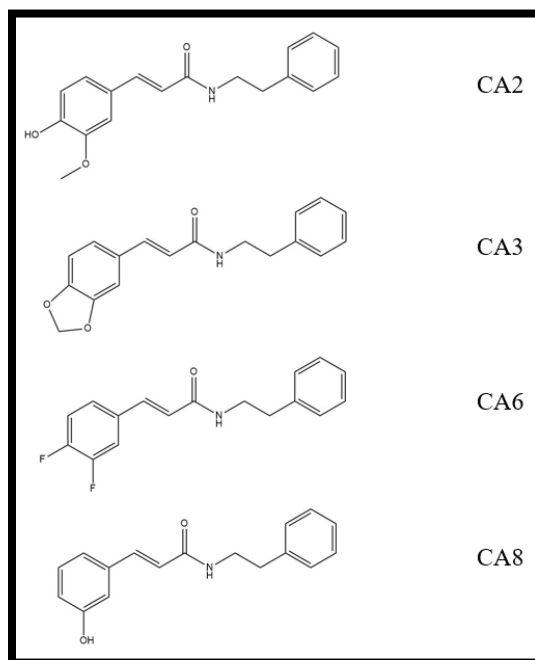
Figure 8: Top 4 analogues determined by affinity in computational docking with 1A9U and 1LEW. The three-character codes will be used to denote each analogue in the graphical representations and score tables
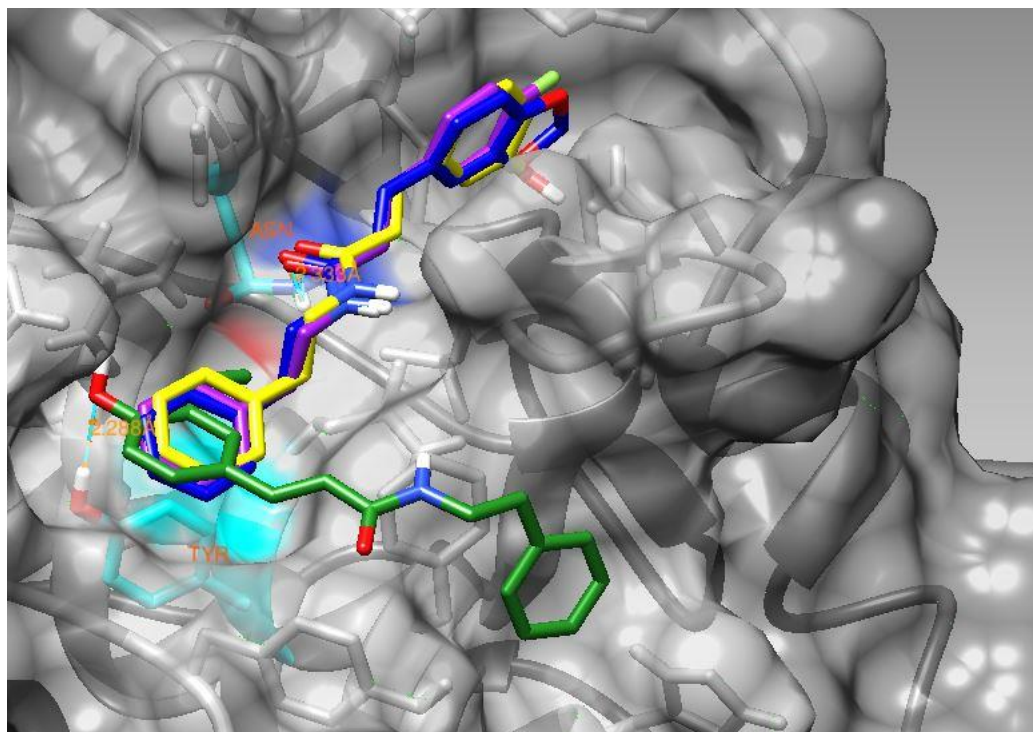
Figure 9: Graphical representation of the four highest affinity CAPA analogue poses docked with the crystal structure of p38α (PDB 1A9U). Each analogue is colored to differentiate between the ligands; Green: CA2, Blue: CA3, Purple: CA6, Yellow: CA8. Hydrogen bonds and residues engaged in hydrogen bonds with the ligands are colored cyan. All residues within 4 Å are shown as stick figures in light gray.

Table 8: Nine poses generated from docking CA2 with the p38α crystal structure (PDB 1A9U) in AutoDock Vina. Affinity is measured by binding energy in kcal/mol. The variability of the poses compared to the highest scored pose is reported as root-mean-square deviation (Å).

mode	affinity (kcal/mol)	dist from best mode rmsd l.b.	rmsd u.b.
1	-7.1	0.000	0.000
2	-6.9	0.964	2.299
3	-6.8	7.214	9.266
4	-6.8	1.278	2.567
5	-6.6	5.652	8.089
6	-6.5	2.769	8.649
7	-6.4	2.788	8.785
8	-6.3	2.552	8.685
9	-6.0	5.268	8.037

The Vanillin based analogue (CA2) has reasonably favorable affinity scores that indicate successful docking. The RMSD values are generally high but two of the major poses are fairly similar to the top scoring pose. The orientation of both the catechol group and the hydrophobic phenyl group is similar to that of the parent CAPA molecule. The hydroxyl group at the para position is engaged in a hydrogen bond with the Tyr 132 residue as previously observed. Notably, the molecule is not inserted into the hydrophobic pocket characteristic of CAPE binding.

Table 9: Nine poses generated from docking CA3 with the p38α crystal structure (PDB 1A9U) in AutoDock Vina. Affinity is measured by binding energy in kcal/mol. The variability of the poses compared to the highest scored pose is reported as root-mean-square deviation (Å).

mode	affinity (kcal/mol)	dist from best mode rmsd l.b.	rmsd u.b.
1	-7.6	0.000	0.000
2	-7.3	2.156	10.058
3	-7.3	0.947	1.483
4	-7.2	2.625	10.091
5	-6.9	3.191	10.920
6	-6.8	3.057	10.950
7	-6.7	7.368	8.919
8	-6.7	6.786	9.388
9	-6.6	7.759	9.502

The piperonal based analogue (CA3) demonstrated the highest affinity for the p38α protein that was observed in any ligand. The RMSD values being generally higher suggests a sampling of many orientations. Despite the high variability of the poses, two of the highest scoring poses were observed to bind in an orientation similar to CAPE. The increased hydrophobicity as a result of the introduction of the dioxolane group may allow the molecule to engage the hydrophobic pocket described previously. Conversely however, when docked with the 1LEW p38α crystal structure the CA3 ligand is found docked more like the CAPA parent compound. These mixed results along with high

RMSD values suggest that the highest affinity pose may not be representative of the

mode of binding in solution.

Table 10: Nine poses generated from docking CA6 with the p38α crystal structure (PDB 1A9U) in AutoDock Vina. Affinity is measured by binding energy in kcal/mol. The variability of the poses compared to the highest scored pose is reported as root-mean-square deviation (Å).

```
mode |   affinity  | dist from best mode
     |  (kcal/mol) | rmsd l.b.| rmsd u.b.
-----+-------------+----------+----------
  1           -7.4      0.000       0.000
  2           -7.3      4.098       9.842
  3           -7.3      4.206       9.910
  4           -7.1      0.919       1.463
  5           -7.0      1.561       2.315
  6           -6.8      4.577       9.866
  7           -6.8      5.165      10.459
  8           -6.7      7.326       8.972
  9           -6.7      4.721       9.873
```

The binding energy for the di-fluoro analogue was determined to be favorable.

Despite having high RMSD values the biding energies are generally favorable the top

five scored poses. Analysis of the graphical representation reveals that, despite the high

polarity of the carbon fluorine bond this analogue the top pose shows the di-fluoro ring

inserted in the hydrophobic pocket. This may be a result of the different electronic

environment created by the fluorine groups compared to the hydroxyls previously

observed. However, only one of the poses is oriented in this way whereas the other poses

show binding more characteristic of CAPA. Several other poses where binding the

hydrophobic pocket is not observed have a very similar binding affinity it is possible that

the top pose while favorable *in silico* is not the major mode of binding.

Table 11: Nine poses generated from docking CA8 with the p38α crystal structure (PDB 1A9U) in AutoDock Vina. Affinity is measured by binding energy in kcal/mol. The variability of the poses compared to the highest scored pose is reported as root-mean-square deviation (Å).

```
mode |   affinity  | dist from best mode
     |  (kcal/mol) | rmsd l.b.| rmsd u.b.
-----+-------------+----------+----------
  1         -7.2       0.000       0.000
  2         -7.0       1.972       9.638
  3         -6.9       2.294       9.634
  4         -6.7       7.332       8.983
  5         -6.7       6.354       9.022
  6         -6.7       7.613      10.292
  7         -6.6       2.321      10.036
  8         -6.6       2.131       3.408
  9         -6.4       6.186       8.892
```

The results of docking the CA8 ligand with p38α revealed the ligand has moderate to high affinity for the protein. The high RMSD values of the bottom eight poses suggest that the top pose, although favorable, is probably not the dominant position of the molecule. The graphical representation reveals that all other poses are oriented differently from the top pose. The positioning of the hydroxyl group in the meta position and the lack of a second hydroxyl group may allow it to enter the hydrophobic pocket, but molecular dynamics studies or *in vitro* analysis would need to be conducted to verify this hypothesis.
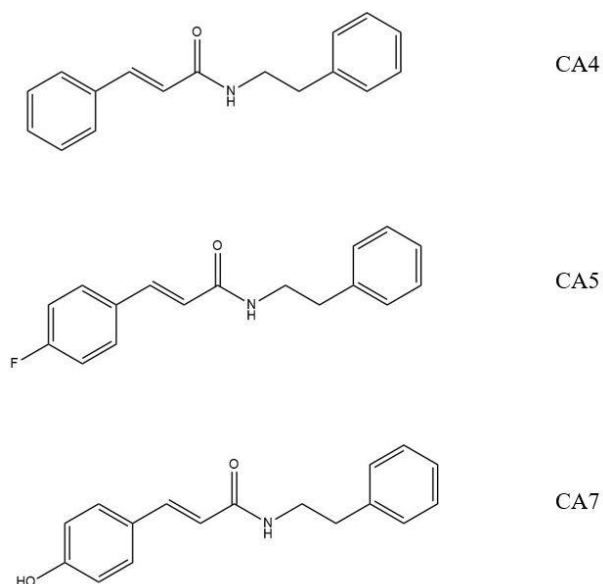
CA4

CA5

CA7

Figure 10: Bottom 3 analogues determined by affinity in computational docking with 1A9U and 1LEW. The three-character codes will be used to denote each analogue in the graphical representations and score tables.

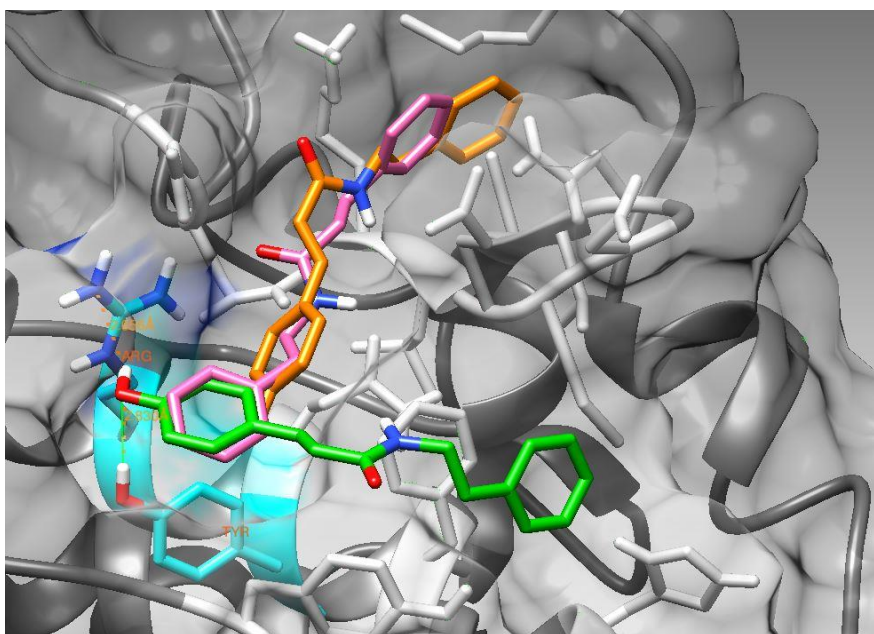**Figure 11:** Graphical representation of the three lowest affinity CAPA analogue poses docked with the crystal structure of p38α (PDB 1A9U). Each analogue is colored to differentiate between the ligands; pink: CA4, orange: CA5, orange: CA7, light green. Hydrogen bonds and residues engaged in hydrogen bonds with the ligands are colored cyan. All residues within 4 Å are shown as stick figures in light gray.

Table 12: Nine poses generated from docking CA4 with the p38α crystal structure (PDB 1A9U) in AutoDock Vina. Affinity is measured by binding energy in kcal/mol. The variability of the poses compared to the highest scored pose is reported as root-mean-square deviation (Å).

```
mode |   affinity  | dist from best mode
     |  (kcal/mol) |  rmsd l.b.| rmsd u.b.
-----+-------------+----------+----------
   1        -6.8       0.000       0.000
   2        -6.8       1.852       9.352
   3        -6.7       1.650       2.907
   4        -6.7       1.704       3.046
   5        -6.6       1.167       9.182
   6        -6.5       1.230       9.477
   7        -6.5       1.464       2.209
   8        -6.5       1.358       9.299
   9        -6.4       6.696       8.477
```

Table 13: Nine poses generated from docking CA5 with the p38α crystal structure (PDB 1A9U) in AutoDock Vina. Affinity is measured by binding energy in kcal/mol. The variability of the poses compared to the highest scored pose is reported as root-mean-square deviation (Å).

```
mode |   affinity  | dist from best mode
     |  (kcal/mol) |  rmsd l.b.| rmsd u.b.
-----+-------------+----------+----------
   1        -7.1       0.000       0.000
   2        -6.9       3.567       9.844
   3        -6.8       3.515       9.207
   4        -6.8       3.533       9.677
   5        -6.7       3.525       9.409
   6        -6.6       2.339       3.940
   7        -6.6       8.540       9.689
   8        -6.6       8.363       9.417
   9        -6.5       3.939       9.934
```

Table 14: Nine poses generated from docking CA7 with the p38α crystal structure (PDB 1A9U) in AutoDock Vina. Affinity is measured by binding energy in kcal/mol. The variability of the poses compared to the highest scored pose is reported as root-mean-square deviation (Å).

```
mode |   affinity  | dist from best mode
     |  (kcal/mol) |  rmsd l.b.| rmsd u.b.
-----+-------------+----------+----------
   1        -6.9       0.000       0.000
   2        -6.9       0.781       1.653
   3        -6.8       8.412       9.602
   4        -6.8       0.095       1.089
   5        -6.8       7.381      10.310
   6        -6.6       6.754       8.235
   7        -6.4       5.977       9.029
   8        -6.3       2.240       8.345
   9        -6.2       2.182       8.413
```

The analogues with the lowest affinity scores were also docked to p38α in an effort to elucidate what structural characteristics can contribute to modes of binding. Analysis of the graphical representation (Fig.11) gives some insight into binding site preference. The ligand with the hydroxyl group in the para position is coordinating with Arg 136 residue and is oriented in the conformation observed with the parent CAPA. The more hydrophobic ligand with a phenyl group on both flanks of the molecule is bound in the hydrophobic pocket despite is structural similarity to CAPA. Taken together these results indicate it may be possible to alter the CAPA mode of mode of binding by changing the substituents of the aromatic ring. With the exception of CA3 all of these findings were reproduced when the ligands were bound to the 1LEW crystal structure of p38α (appendix Fig.18). To validate our findings, we need to conduct molecular dynamics studies on these ligands with p38α to see if their top scores are representative of their binding activity or if the high upper bound RMSD values truly suggest an unstable interaction.

3.3. Future Directions:

The computational docking result gathered in this study have given us insight into how the biological activity of CAPA may differ from that of the parent CAPE. Specifically, on why Li. et al. observed a difference in the ability of CAPA to bind to p38α. This work has served to validate the previous experimental observations and allowed us to form a hypothesis as to why only CAPE seems to be capable of binding to the DRS of p38α. If binding of the hydrophobic pocket is exclusive to CAPE and only CAPE demonstrates an inhibitory effect, then binding in this pocket may have an

allosteric effect on p38α. The observations described in this work are promising but further work will need to be done to validate our findings. Molecular dynamics studies will serve to verify if CAPE is strongly binding to the highly specific DRS. Additionally, *in vitro* binding studies should be conducted on CAPE, CAPA, and its analogues. This will serve to validate the preliminary *in silico* findings described in this work. Both of these techniques will also be applied to the CAPA analogues to further explore how changing the catechol group may impact the biological activity of CAPE/CAPA.

The molecules synthesized in this study along with several others will be screened for activity in cancer cell lines. We will be incubating cancer cell lines with these small molecules and observer the survivability of these cells. This will be done in neuroblastoma and multiple myeloma cell lines and ideally, any of the types of cancer that CAPE is active in. Lastly, the molecules synthesized here will be exposed to an *in vitro* phase II metabolism assay using minipig microsomes. This will allow us to determine how changing the substituents of the phenyl rings in CAPA mediate drug permanence.
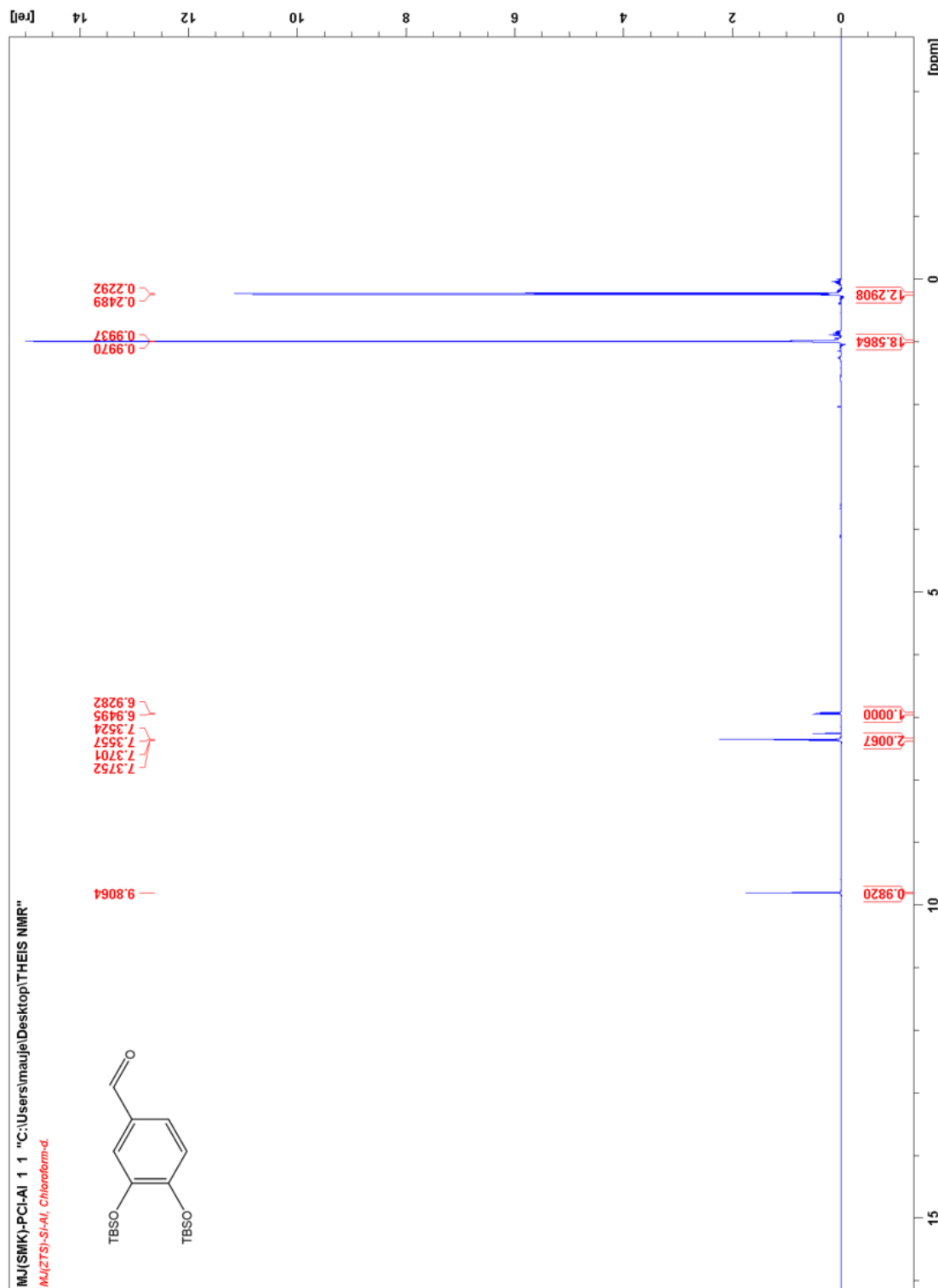
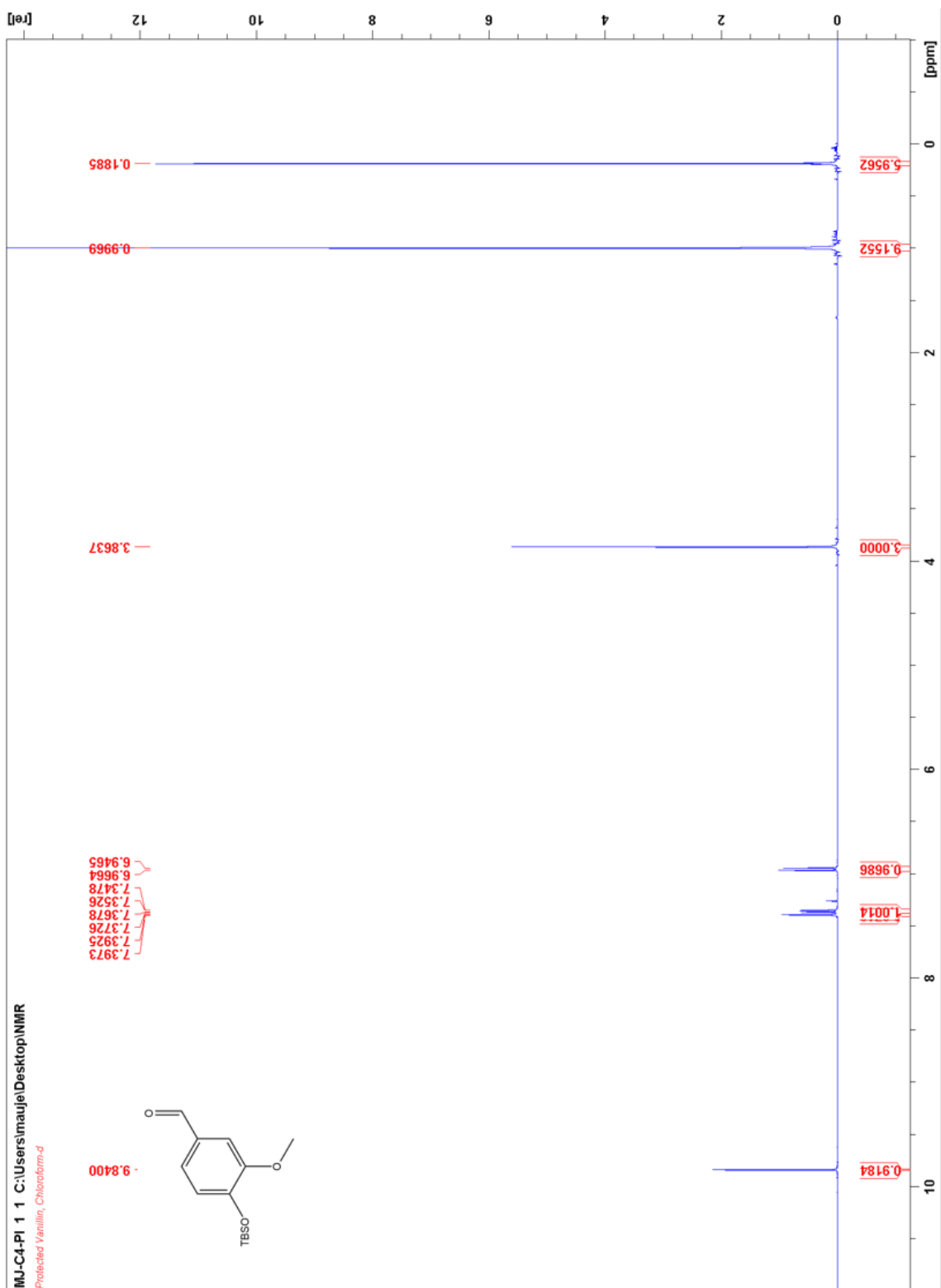**Fig.1: ¹H NMR of 3,4-Bis-((ter-butyldimethyl-silyl)oxy)benzaldehyde (2a) in CDCl₃**

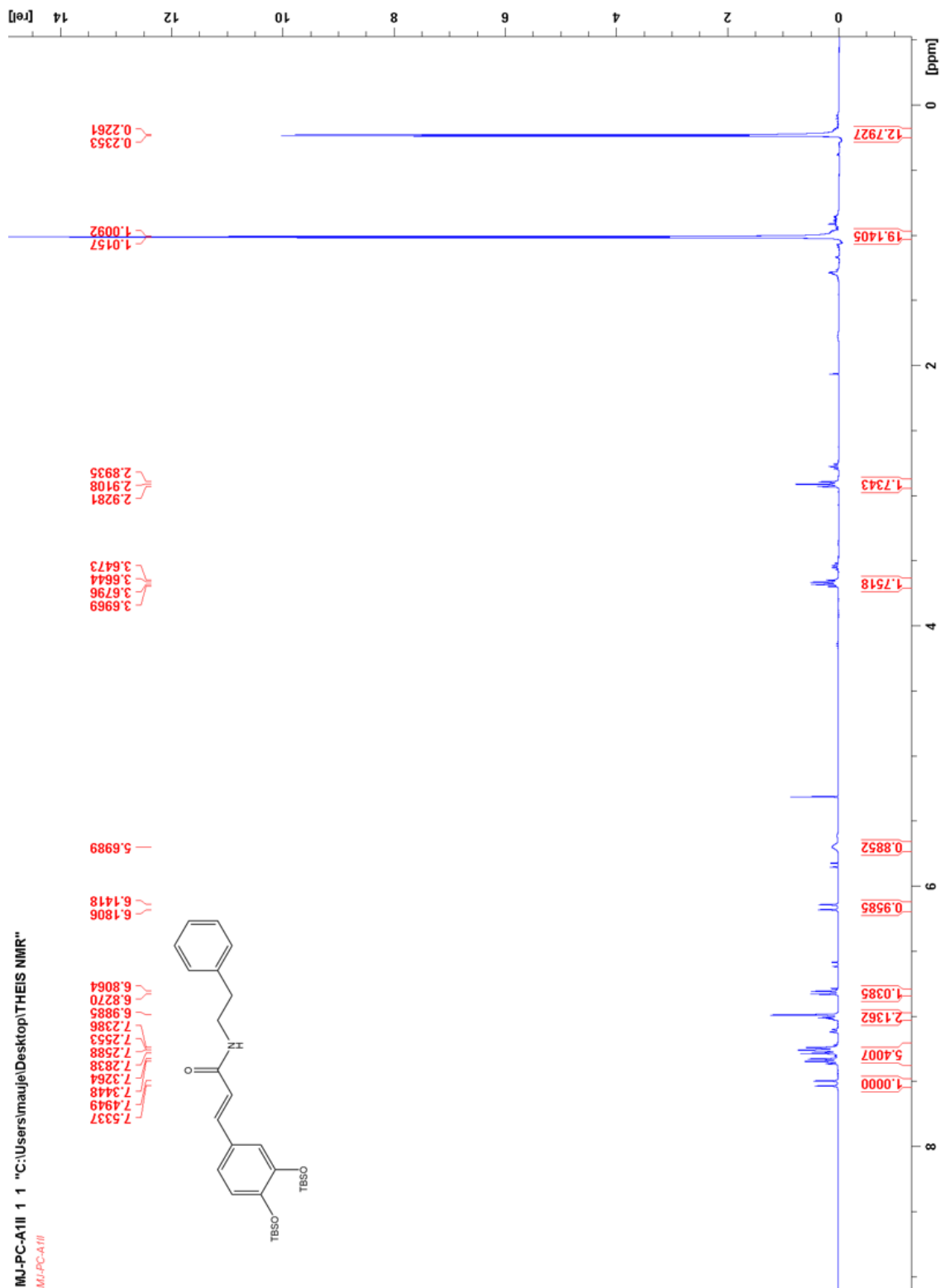**Fig.2: ¹H NMR 4-{[Dimethyl(2-methyl-2-propanyl)silyl]oxy}-3-methoxybenzaldehyde (2b) in CDCl₃**

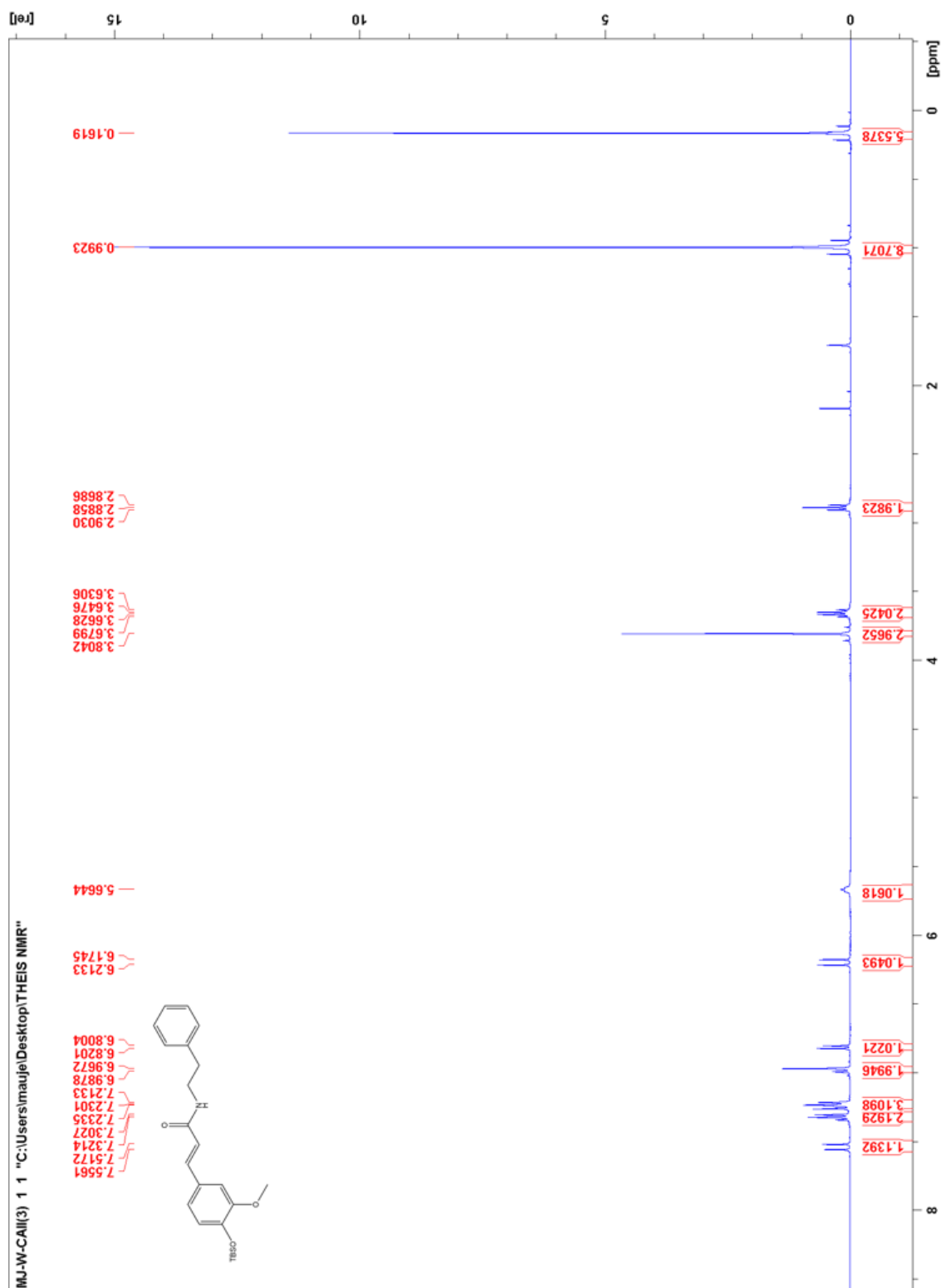**Fig.3: ¹H NMR *E*)-3-(3,4-bis((tert-butyldimethylsilyl)oxy)phenyl)-*N*-phenethylacrylamide (3a) in CDCl₃**

Fig.4: ^{1}H NMR (2*E*)-3-((4- tert-butyldimethylsilyl)oxy)-3-methoxyphenyl)-*N*-(2-phenylethyl)acrylamide (3b) in CDCl$_3$
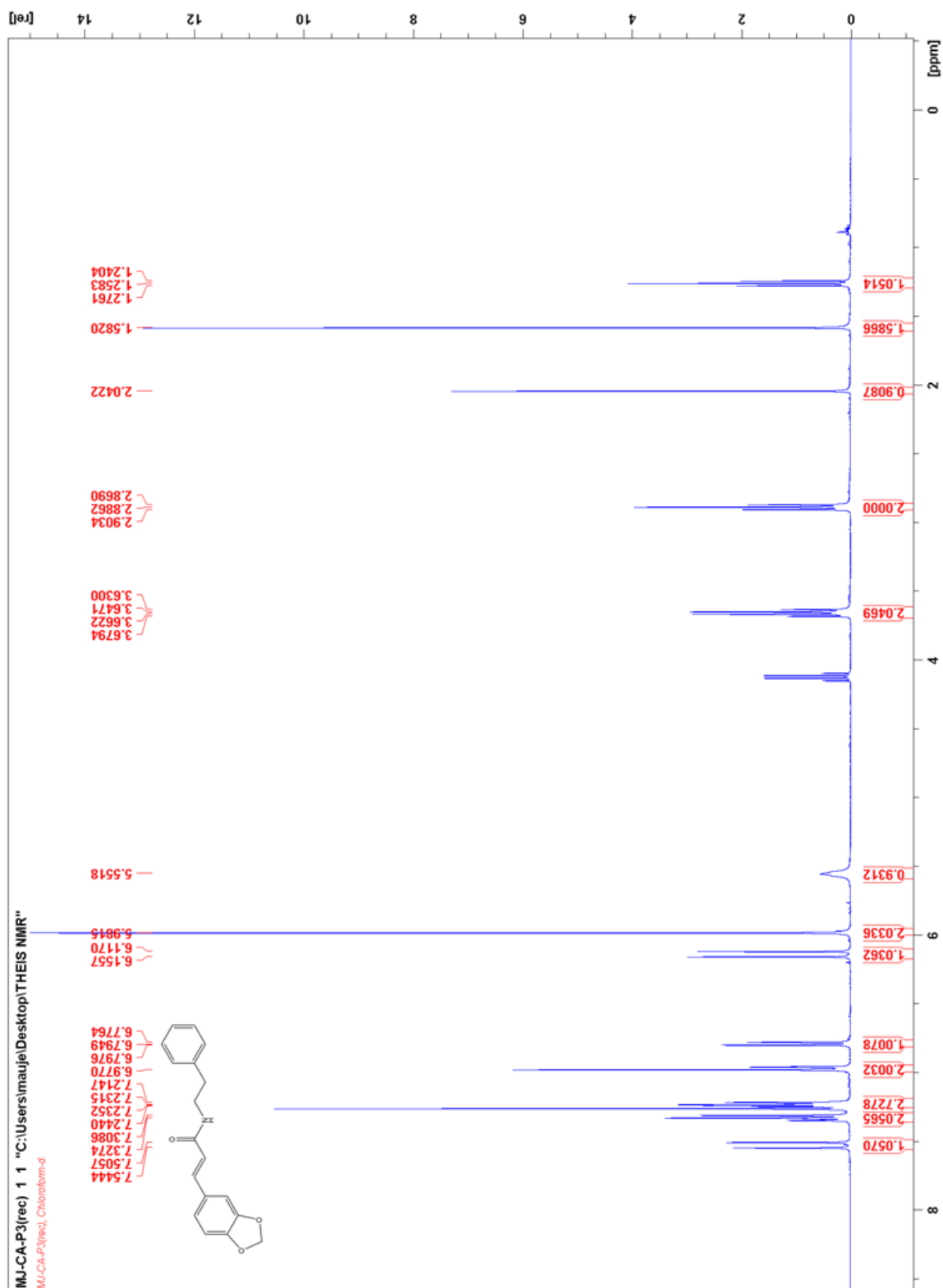
Fig.5: ¹H NMR (2*E*)-3-(1,3-Benzodioxol-5-yl)-*N*-(2-phenylethyl)acrylamide (3c) acetone-d6
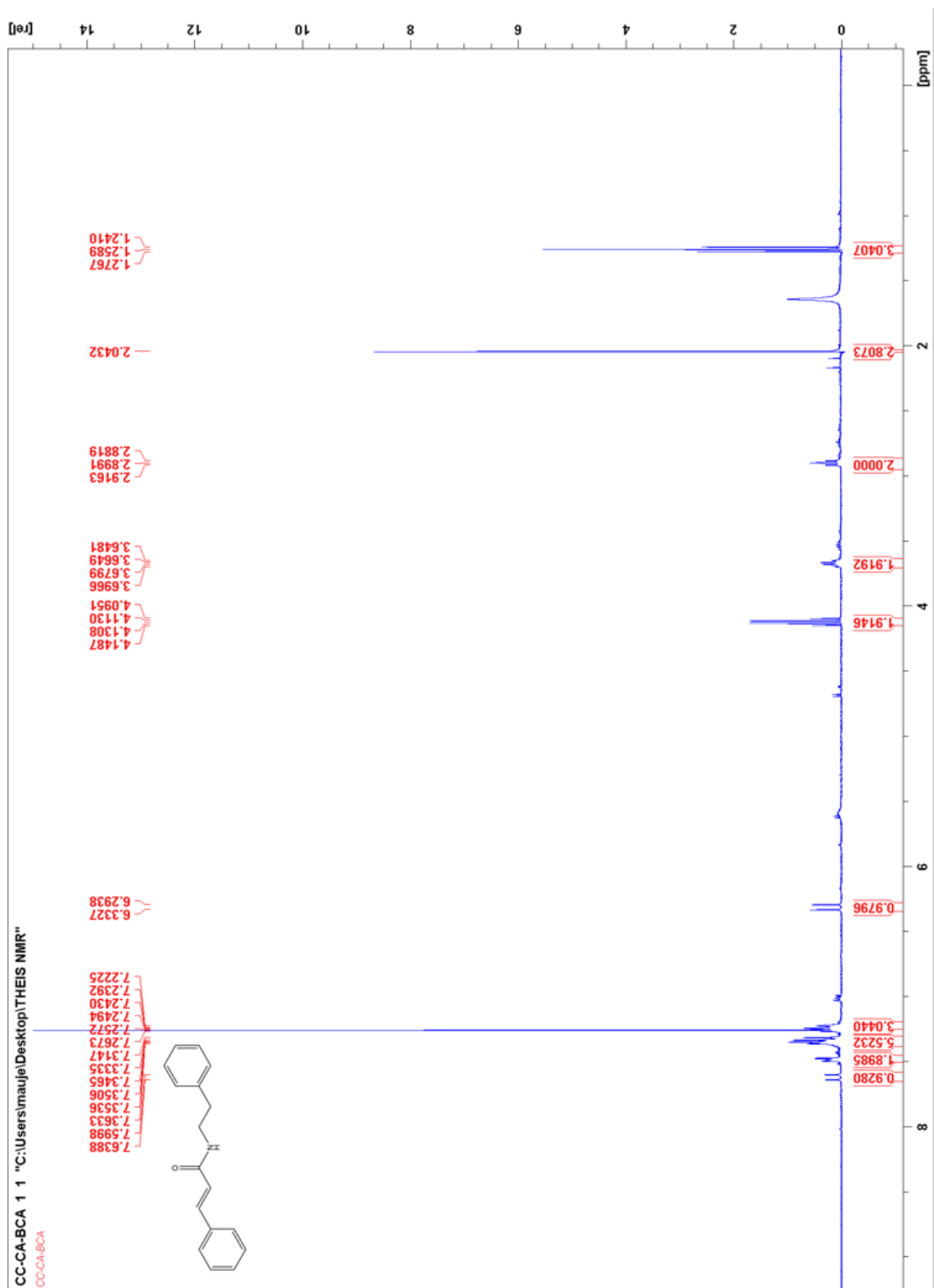
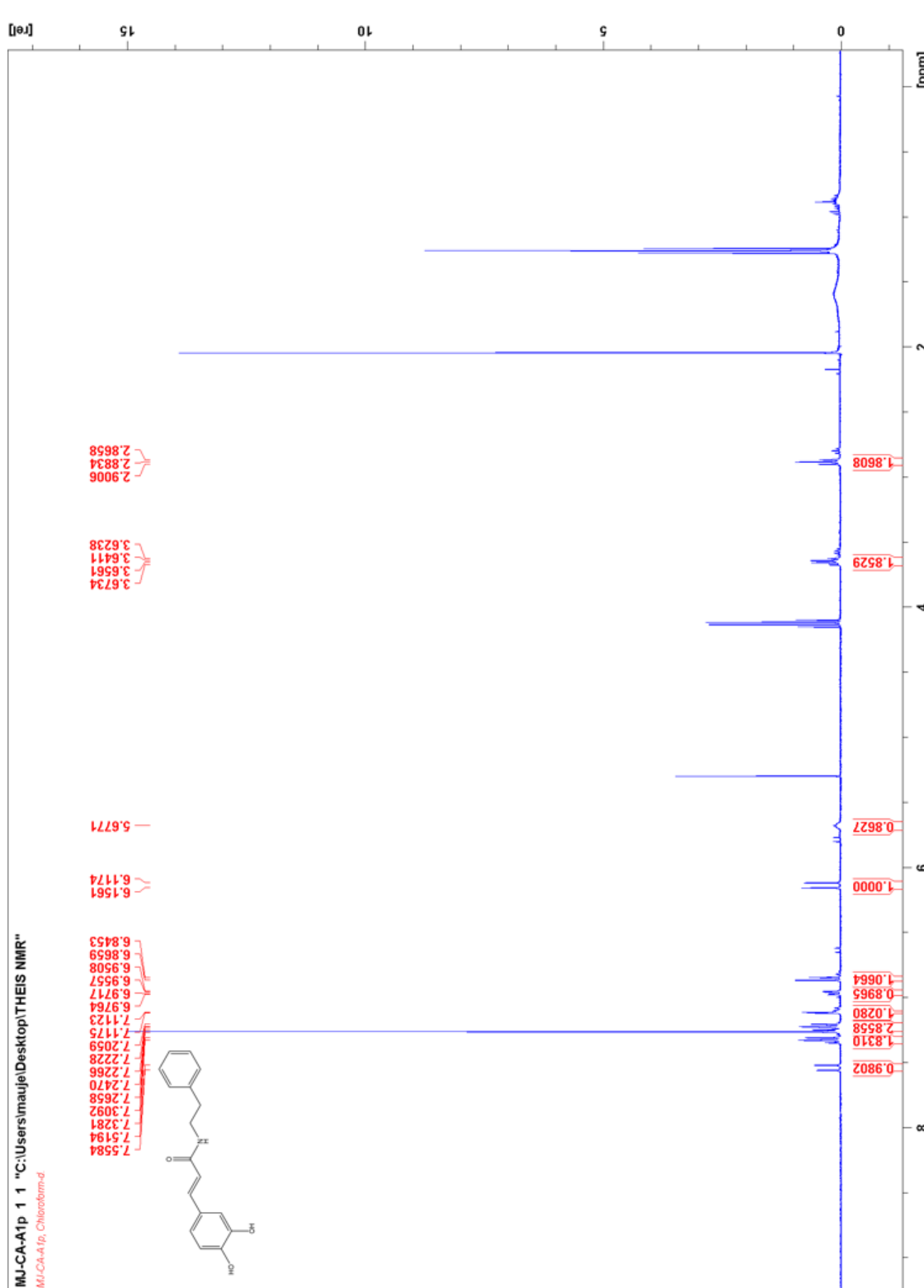**Fig. 6: ¹H NMR (2*E*)-3-Phenyl-*N*-(2-phenylethyl)-2-propenamide (3d) in CDCl₃**

Fig.7: ¹H NMR (2*E*)-3-(3,4-Dihydroxyphenyl)-*N*-(2-phenylethyl)acrylamide (4a) in CDCl₃

MJ-CA-P2 1 1 "C:\Users\mauje\Desktop\THEIS NMR"

MJ-CA-P2

[rel]

15   10   5   0   [ppm]

1.1877
1.1877
1.2055
1.2233

2.9882

3.5469
3.5621
3.5656
3.5776
3.5804
3.5820
3.5852
3.5984
3.8636

6.5144
6.5535
6.8421
6.8625
7.0418
7.0461
7.0622
7.0671
7.1559
7.1607
7.2437
7.2598
7.2649
7.2673
7.2691
7.2841
7.2860
7.3541
7.4759
7.5149

2.0331
1.0481
1.9925
3.0233
1.0000
1.0109
1.0596
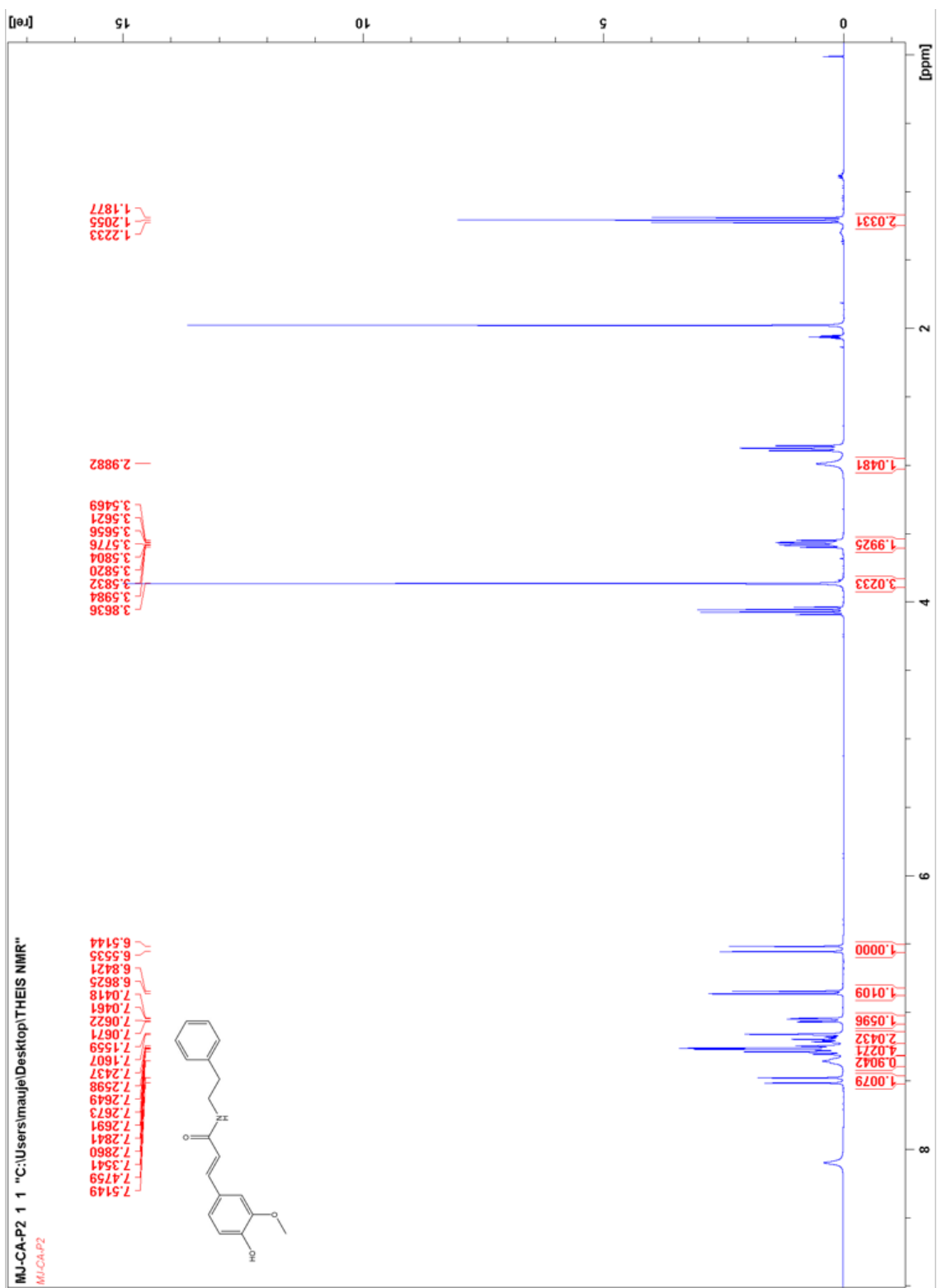2.0432
4.0221
0.9042
1.0079

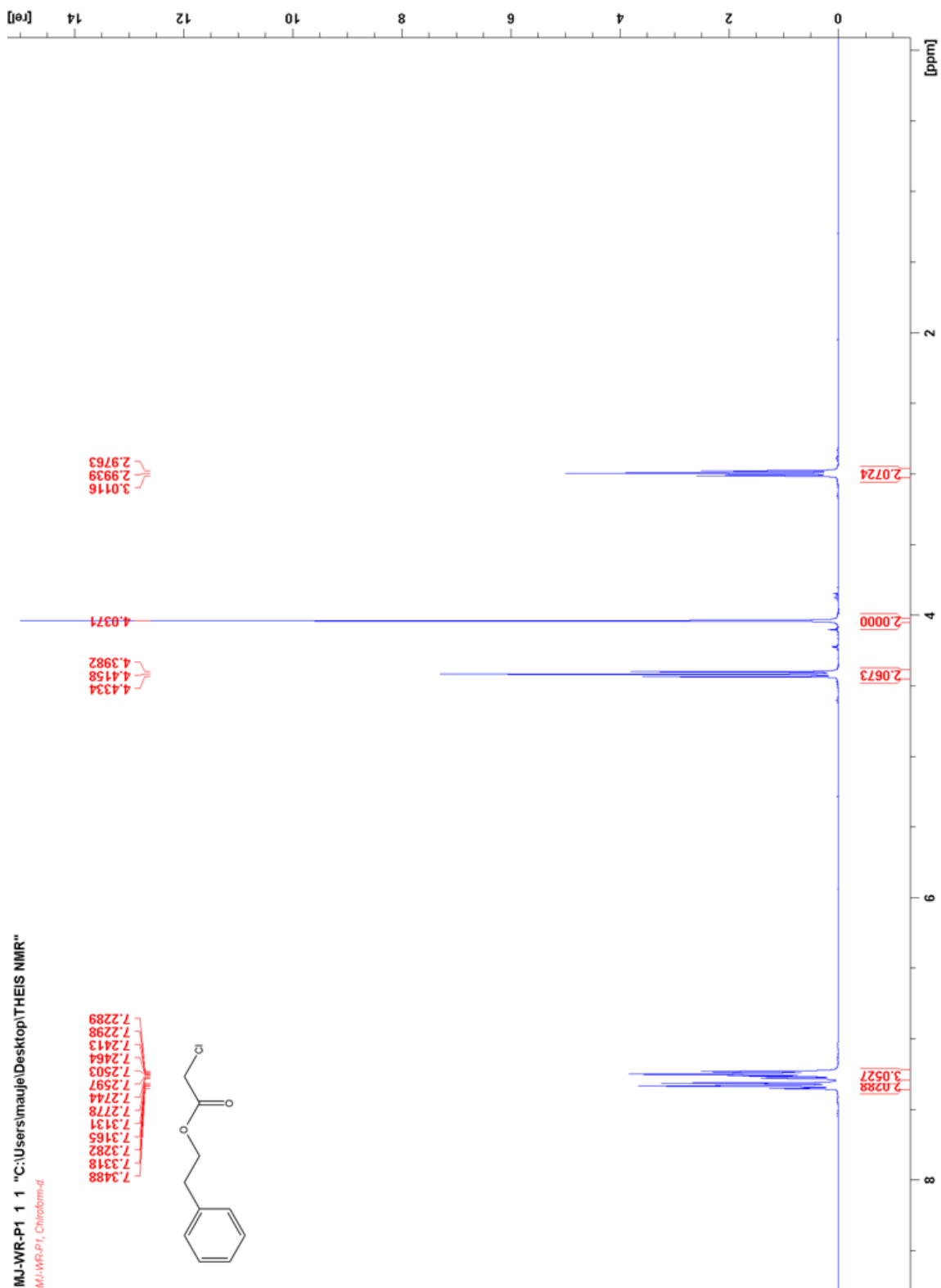Fig.8: ¹H NMR (2*E*)-3-(4-Hydroxy-3-methoxyphenyl)-*N*-(2-phenylethyl)acrylamide (4b) in CDCl₃

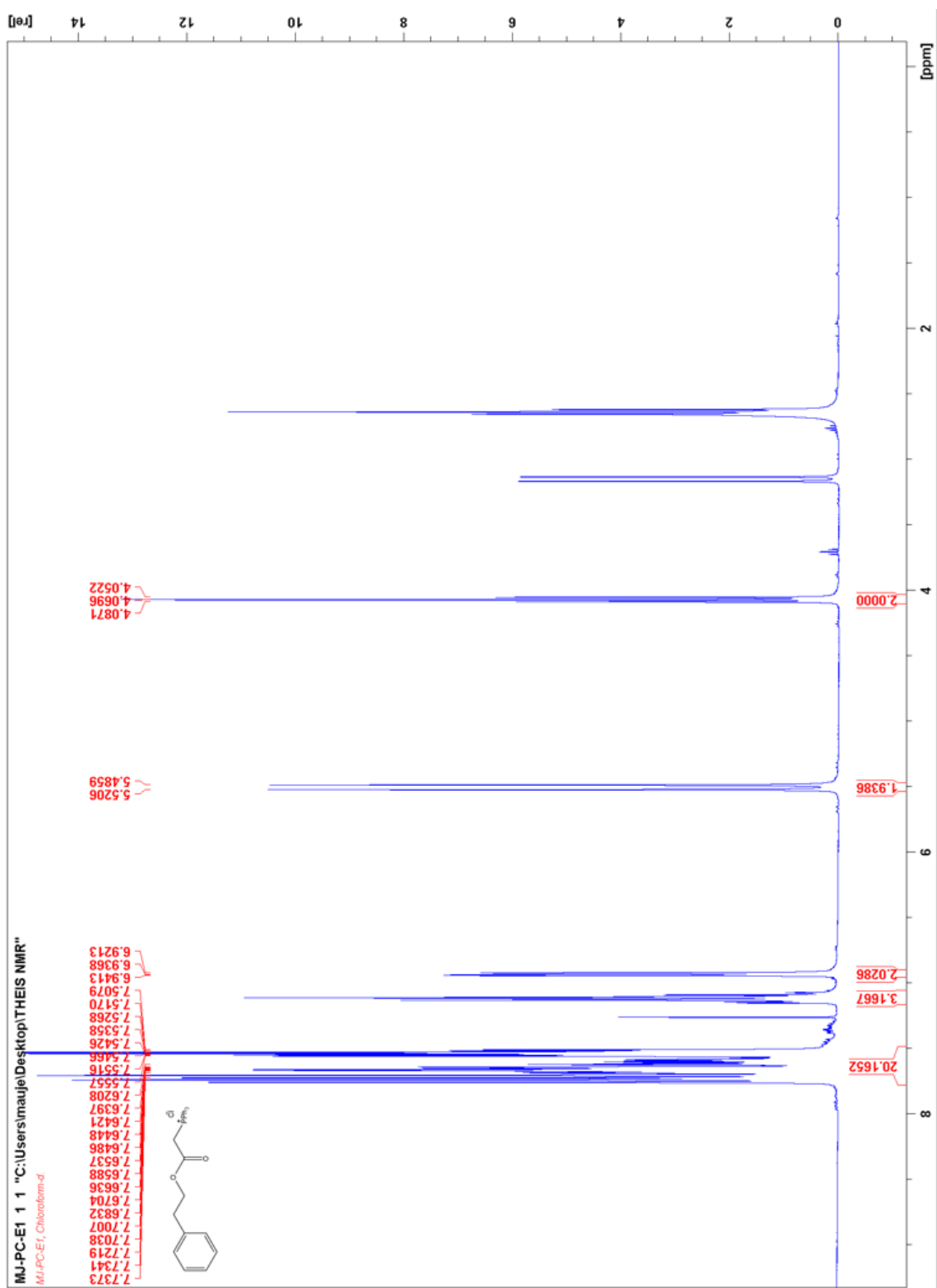**Fig.9: ¹H NMR 2-Phenylethyl chloroacetate (5) in CDCl₃**

Fig.10: ^{1}H NMR Phenethyloxycarbonylmethyl-triphenyl-phosphonium chloride (6) in CDCl$_3$
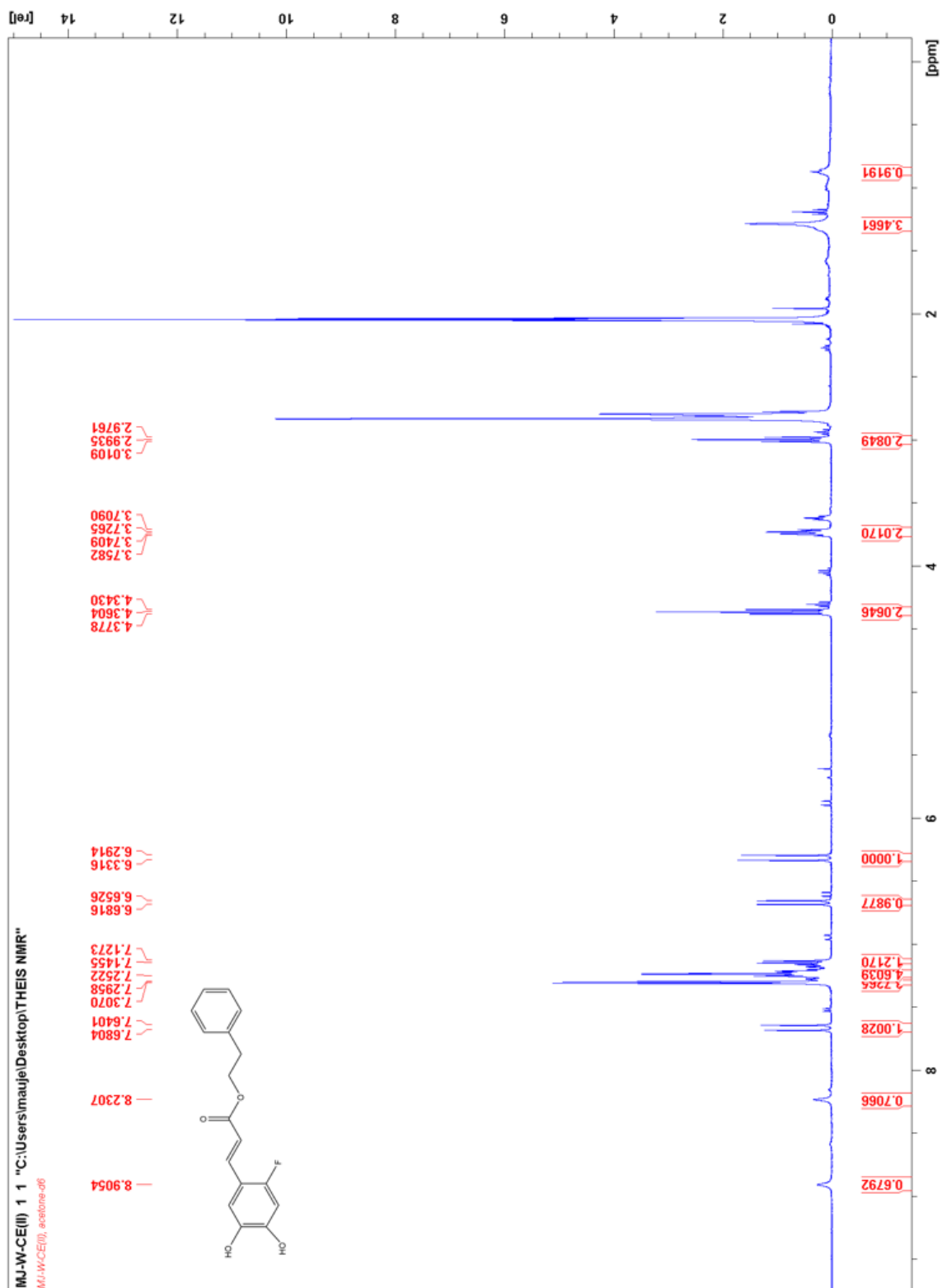
Fig.11: ^{1}H NMR 2-Phenylethyl (*2E*)-3-(2-fluoro-4,5-dihydroxyphenyl)acrylate (7) in CDCl₃
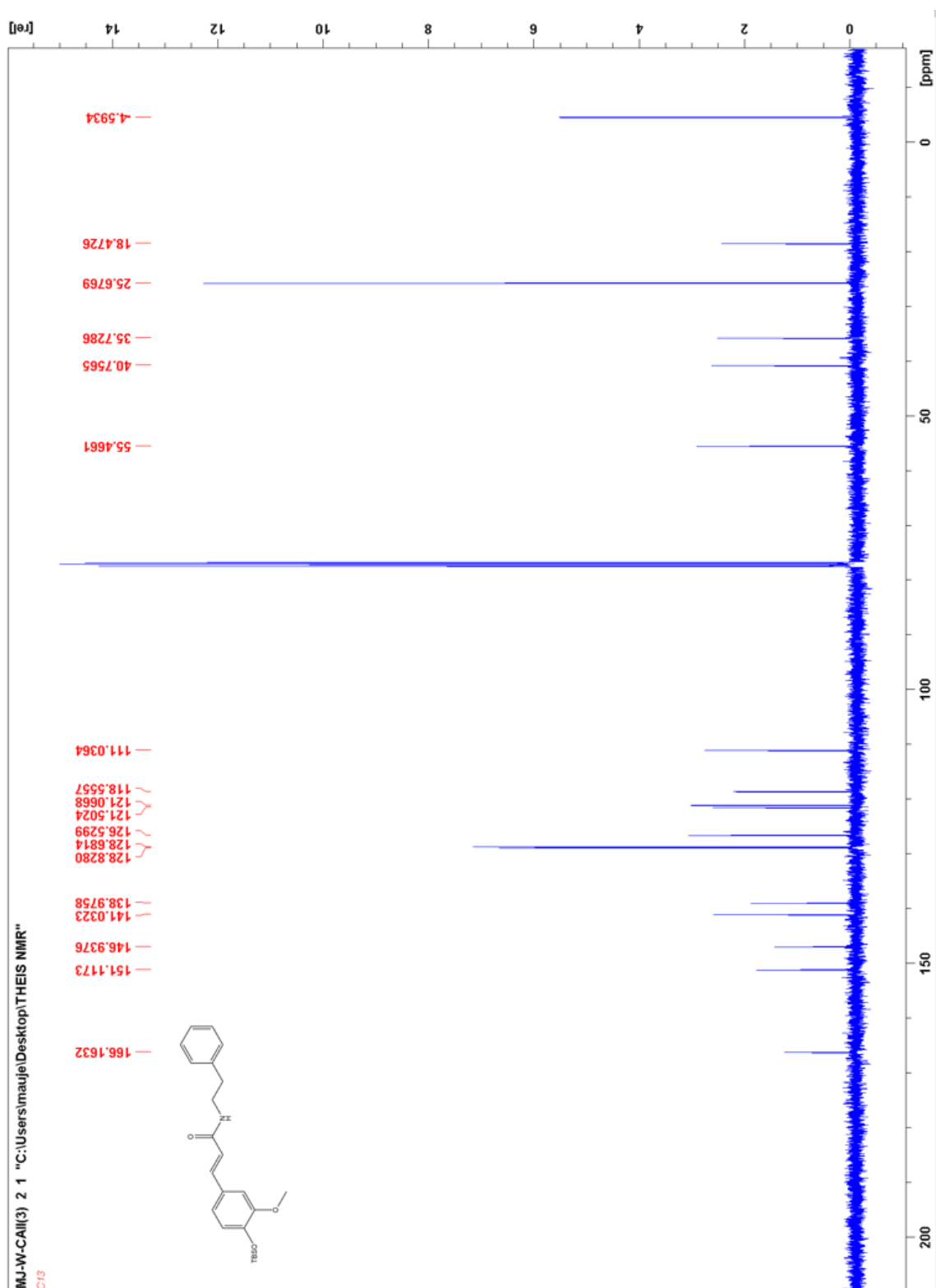
Fig.12: ^{13}C NMR (2*E*)-3-((4- tert-butyldimethylsilyl)oxy)-3-methoxyphenyl)-*N*-(2-phenylethyl)acrylamide (3b) in CDCl₃
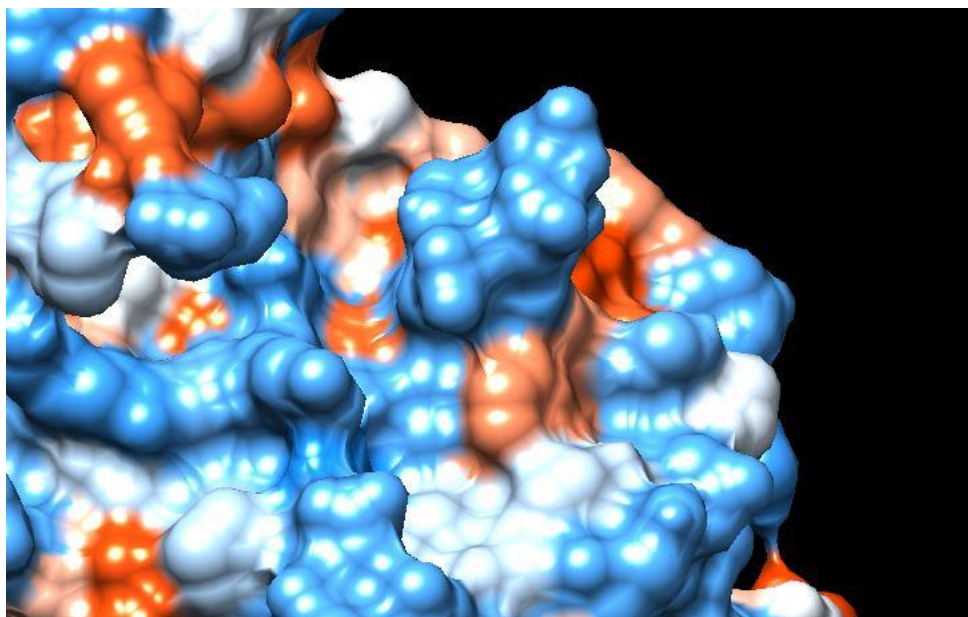
Fig. 13: Surface hydrophobicity of p38a (PDB 1A9U)

Fig. 14: Graphical representation of all CAPE poses docked with p38a (PDB 1A9U)
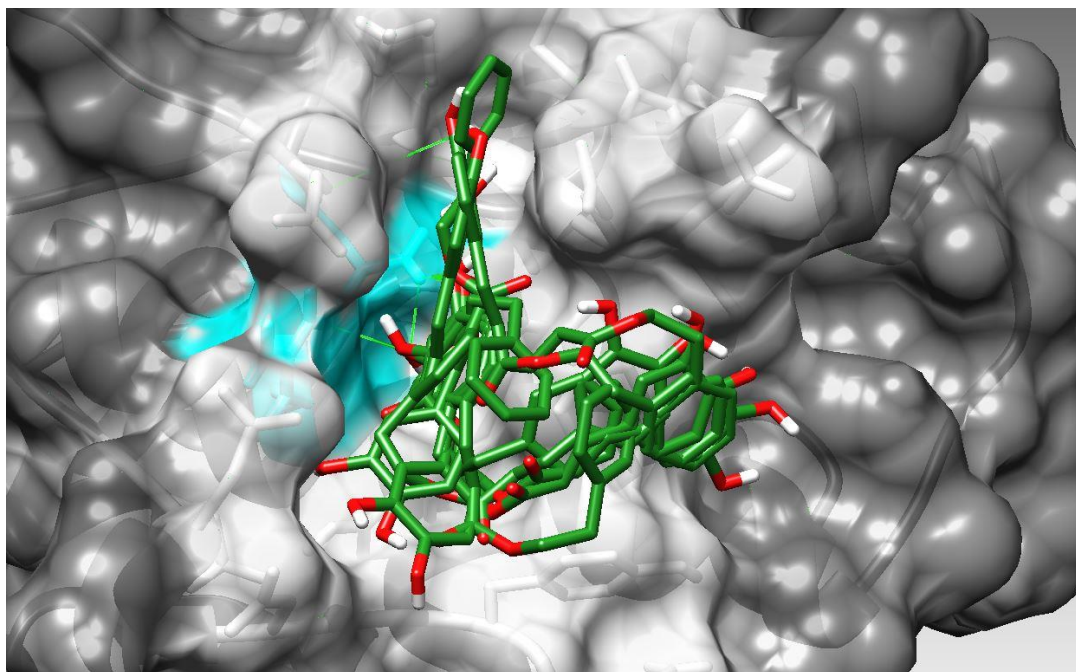
Fig. 15: Graphical representation of all CAPE poses docked with p38a (PDB 1LEW)
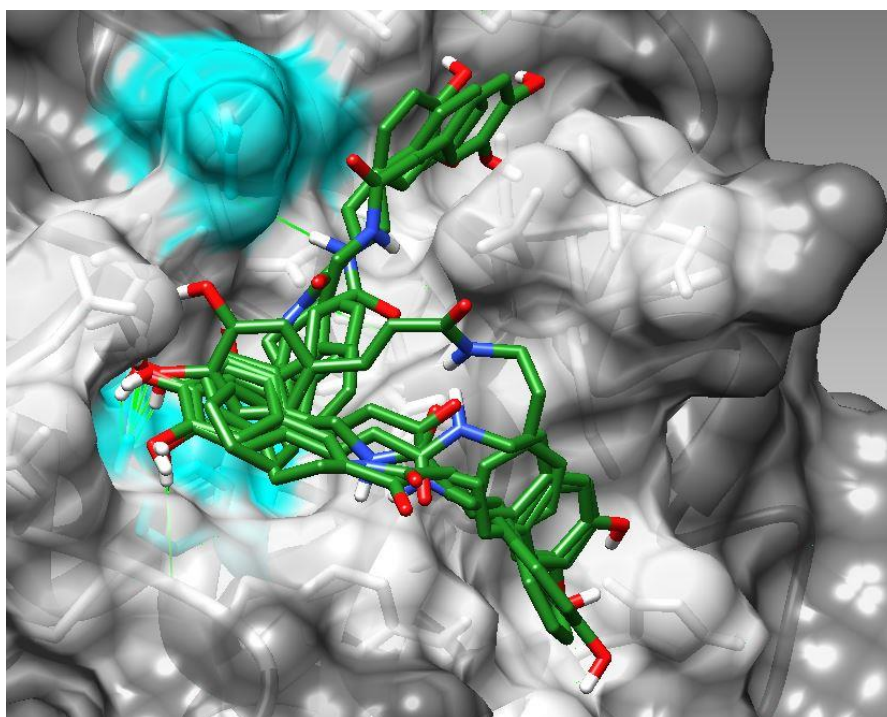
Fig. 16: Graphical representation of all CAPA poses docked with p38a (PDB 1A9U)
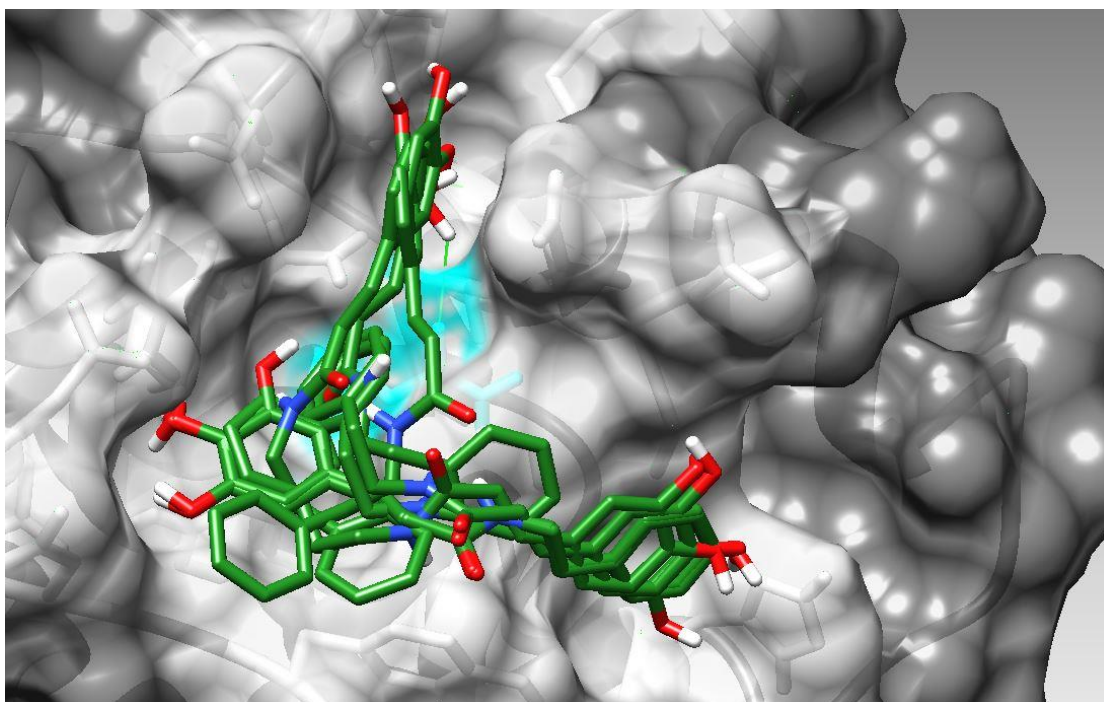
Fig. 17: Graphical representation of all CAPA poses docked with p38a (PDB 1LEW)
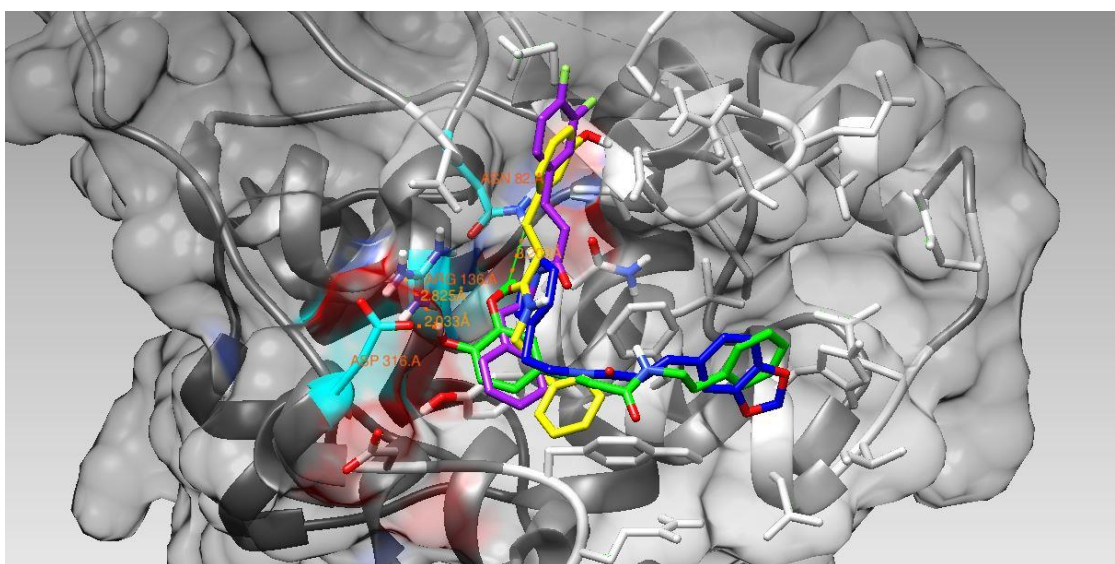
Fig. 18: Graphical representation of the top 4 scoring CAPA analogues docked with p38a (PDB 1LEW)

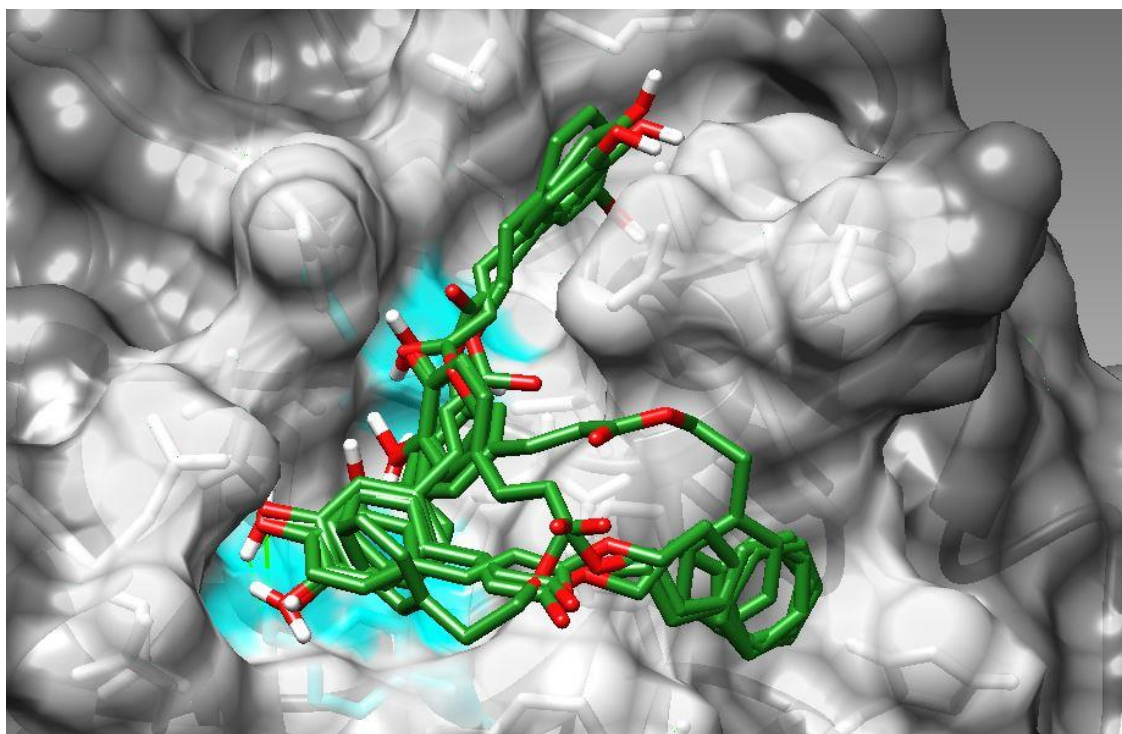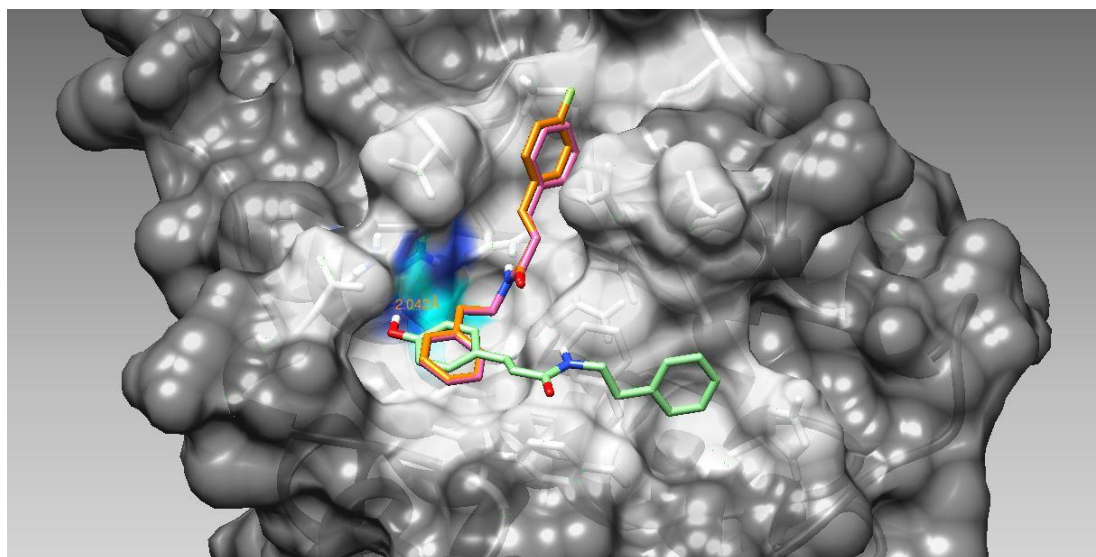**Fig. 19: Graphical representation of the bottom 3 scoring CAPA analogues docked with p38a (PDB 1LEW)**

Table 1: Scores for CA2 docked with 1LEW

mode	affinity (kcal/mol)	dist from best mode rmsd l.b.	rmsd u.b.
1	-6.9	0.000	0.000
2	-6.6	1.272	2.541
3	-6.4	2.749	8.996
4	-6.3	2.872	9.282
5	-6.2	2.726	8.845
6	-6.1	1.843	2.613
7	-6.1	5.988	9.031
8	-6.1	2.808	3.999
9	-6.0	3.145	4.045

Table 2: Scores for CA3 docked with 1LEW

```
mode |   affinity | dist from best mode
     | (kcal/mol) | rmsd l.b.| rmsd u.b.
-----+------------+----------+----------
   1       -7.1       0.000       0.000
   2       -7.1       5.891       9.401
   3       -6.9       1.336       2.343
   4       -6.9       6.118       8.314
   5       -6.8       1.054       1.514
   6       -6.7       6.059       8.373
   7       -6.7       1.361       1.886
   8       -6.7       6.562       9.490
   9       -6.7       1.484       2.452
```

Table 3: Scores for CA6 docked with 1LEW

```
mode |   affinity | dist from best mode
     | (kcal/mol) | rmsd l.b.| rmsd u.b.
-----+------------+----------+----------
   1       -7.0       0.000       0.000
   2       -6.8       1.550       2.284
   3       -6.7       4.748       9.666
   4       -6.6       2.587       3.224
   5       -6.6       6.748       9.011
   6       -6.6       6.950       9.867
   7       -6.6       1.595       2.383
   8       -6.6       7.340       9.856
   9       -6.5       6.568       8.669
```

Table 4: Scores for CA8 docked with 1LEW

```
mode |   affinity | dist from best mode
     | (kcal/mol) | rmsd l.b.| rmsd u.b.
-----+------------+----------+----------
   1       -6.7       0.000       0.000
   2       -6.7       1.957       2.840
   3       -6.6       2.204       3.369
   4       -6.6       1.431       1.867
   5       -6.4       1.628       2.193
   6       -6.4       4.426       7.835
   7       -6.4       5.008       8.407
   8       -6.4       5.121       8.414
   9       -6.4       5.291       8.046
```

Table 5: Scores for CA4 docked with 1LEW

mode	affinity (kcal/mol)	dist from best mode rmsd l.b.	rmsd u.b.
1	-6.7	0.000	0.000
2	-6.5	1.555	2.239
3	-6.5	1.160	8.896
4	-6.3	3.819	7.057
5	-6.3	4.762	7.587
6	-6.3	1.351	1.939
7	-6.2	5.607	8.124
8	-6.2	5.126	8.597
9	-6.2	3.793	6.960

Table 6: Scores for CA5 docked with 1LEW

mode	affinity (kcal/mol)	dist from best mode rmsd l.b.	rmsd u.b.
1	-6.9	0.000	0.000
2	-6.8	0.073	1.539
3	-6.6	3.812	9.453
4	-6.4	6.880	9.382
5	-6.4	5.254	7.844
6	-6.4	6.448	9.434
7	-6.4	5.893	8.342
8	-6.3	5.921	8.361
9	-6.3	6.090	8.195

Table 7: Scores for CA7 docked with 1LEW

mode	affinity (kcal/mol)	dist from best mode rmsd l.b.	rmsd u.b.
1	-6.7	0.000	0.000
2	-6.7	0.140	1.541
3	-6.7	6.230	9.275
4	-6.3	2.358	8.641
5	-6.2	2.547	8.753
6	-6.2	2.524	8.349
7	-6.1	2.652	8.905
8	-6.0	2.338	9.169
9	-5.9	2.281	8.444

REFERENCES

1. Castaldo, S., Capasso, F. (2002) Propolis, an old remedy used in modern medicine. *Fitoterapia, 7: S1-S6.*

2. Boudreau, L., Maillet, J., LeBlanc, Luc., Touaibia, Mohamed, T., Flamand, N., Surette, M. (2012) Caffeic Acid Phenethyl Ester and Its Amide Analogue Are Potent Inhibitors of Leukotriene Biosynthesis in Human Polymorphonuclear Leukocytes. *PLoS ONE, 7(2):1-8.*

3. Wu, J., Omene, C., Karkoszka1, J., Bosland1, M., Eckard, J., Klein, C., Frenkel, K. (2011) Caffeic Acid Phenethyl Ester (CAPE), Derived from a Honeybee Product Propolis, Exhibits a Diversity of Anti-tumor Effects in Preclinical Models of Human Breast Cancer. *Cancer Lett.,* 308(1): 43–53.

4. Wang, X. Stavchansky, S. Bowman, P., Kerwin, S. (2006) Cytoprotective Effect of Caffeic Acid Phenethyl Ester (CAPE) and Catechol Ring-Fluorinated CAPE Derivatives Against Menadione-Induced Oxidative Stress in Human Endothelial Cells *Bioorg. Med. Chem.,* 14:4879-87.

5. Chen, Y., Shiao, M., Hsu, M., Tsai, T., Wang, S. (2001) Effect of Caffeic Acid Phenethyl Ester, an Antioxidant from Propolis, on Inducing Apoptosis in Human Leukemic HL-60 Cells. *J. Agric. Food Chem.,* 49: 5615−5619.

6. Khoram, N., Bigdeli, B., Nikoofar, A., Goliaei, B. (2016) Caffeic Acid Phenethyl Ester Increases Radiosensitivity of Estrogen Receptor Positive and Negative Breast Cancer Cells by Prolonging Radiation-Induced DNA Damage *J. Breast Cancer,* 19(1): 18-25.

7. Marin, E., Paek, H., Li, M., Ban, Y., Karaga, M., Shashidharamurthy, R., Wang, X. (2019) Caffeic acid phenethyl ester exerts apoptotic and oxidative stress on human multiple myeloma cells. *Invest.New Drugs.* 1-12.

8. Fırat, F., Özgül, M., Türköz Uluer E., Inan, S. (2019) Effects of caffeic acid phenethyl ester (CAPE) on angiogenesis, apoptosis and oxidative stress in various cancer cell lines. *Biotechnic & Histochemistry.* 1473-7760.

9. Ahn, M., Kunimasa, K., Kumazawa1, S., Nakayama, T., Kaji, K., Uto, Y., Hori, H., Nagasawa, H., Ohta, T. (2009) Correlation between antiangiogenic activity and antioxidant activity of various components from propolis. *Mol. Nutr. Food Res*. 53: 643–651.

10. Li, J., Kaoud, T.S., Levieux, J., Gilbreath, B., Moharana, S., Dalby, K.N., Kerwin, S.M., 2013. A Fluorescence-Based Assay for p38α Recruitment Site Binders: Identification of Rooperol as a Novel p38α Kinase Inhibitor. (2013) *Chem. Bio. Chem.,* 14: 66-71

11. Wang, X., Bowman, P., Kerwin, S., Stavchansky, S. (2007) Stability of caffeic acid phenethyl ester and its fluorinated derivative in rat plasma. *Biomed. Chromatogr*. 21: 343–350.

12. Wang, X., Pang, J., Maffucci, J., Pade, D., Newman R., Kerwin S., Bowman PD., Stavchansky S. (2009) Pharmacokinetics of caffeic acid phenethyl ester and its catechol-ring fluorinated derivative following intravenous administration to rats. Biopharm Drug Dispos. 30(5): 221-8

13. Yang, J., Kerwin, S., Bowman, P., Stavchansky, S. (2011) Stability of Caffeic Acid Phenethyl Amide (CAPA) in Rat Plasma. *Biomed. Chromatogr*. 26: 594–598.

14. Yang, J., Bowmanb, P., Kerwin, S., Stavchansky, S. (2013) Development and validation of an LCMS method to determine the pharmacokinetic profiles of caffeic acid phenethyl amide and caffeic acid phenethyl ester in male Sprague–Dawley rats. *Biomed. Chromatogr*. 28: 241–246.

15. Yang, J,. Marriner, G., Wang, X., Bowman, P., Kerwin, S., Stavchansky, S. (2010) Synthesis of a series of caffeic acid phenethyl amide (CAPA) fluorinated derivatives: Comparison of cytoprotective effects to caffeic acid phenethyl ester (CAPE). *Bioorganic & Medicinal Chemistry.* 18: 5032–5038.

16. Chen, Z., Gibson, T., Robinson, F., Silvestro, L., Pearson, G., Xu, B., Wright, A., Vanderbilt, Cobb, M., MAP Kinases. Chemical Reviews, 2001. 101(8): 2449-2476.

17. Manning, G., Whyte, D. B., Martinez, R., Hunter, T., Sudarsanam, S. (2002) The Protein Kinase Complement of the Human Genome. *AAAS*. 298: 1912-34.

18. Dhillon, A. S., Hagan, S., Rath, O., Kolch, W. (2007) MAP kinase signalling pathways in cancer. *Oncogene.* 26: 3279-90.

19. Peti, W., Page, R. (2013) Molecular basis of MAP kinase regulation. *Protein Sci.* 12: 1698-1710.

20. Roux, P., Blenis, J., (2004) ERK and p38 MAPK-Activated Protein Kinases: A Family of Protein Kinases with Diverse Biological Functions. *Micro. Bio. & Mol. Bio. Rev.* 2: 320-344.

21. Ono, K., Han. J., (2000) The p38 signal transduction pathway Activation and function. *Cell. Signaling.* 1: 1-13.

22. Hancock, C., Macias, A., Lee, E., Yu, S., MacKerell, D., Shapiro, P., (2005) Identification of Novel Extracellular Signal-Regulated Kinase Docking Domain Inhibitors. *Journal of Medicinal Chemistry* 48 (14), 4586-4595.

23. De, S., Stebbins, J., Chen, L., Riel-Mehan, M., Machleidt, T., Dahl, R., Yuan, H., Aras, E., Barile, E., Chen, V., Murphy, Ria., Pellecchia, M. (2009) Design, Synthesis, and Structure−Activity Relationship of Substrate Competitive, Selective, and in Vivo Active Triazole and Thiadiazole Inhibitors of the c-Jun N-Terminal Kinase. *Journal of Medicinal Chemistry,* 52(7): 1943-1952.

24. Bankova, V. S.J. (1990) Synthesis of Natural Esters of Substituted Cinnamic Acids. *Nat. Prod*. 53: 821–824.

25. Tsubouchi, A. Thioacetalization of Carbonyl Compounds with Metal Salt Based Lewis Acid Catalysts (2016), *Science of Synthesis Knowledge Updates*, 2, 329.

26. Tomas, M.B., Shiao, T.C., Nguyen, P.T., Bourgault, S., Roy, R., (2018) Synthesis of Analogs of Trans-Fagaramide and Their Cytotoxic Activity. *Pharm. Chem. J.* 51: 995–1004.

27. Tseng CF, Iwakami S, Mikajiri A. (1992) Inhibition of in vitro prostaglandin and leukotriene biosyntheses by cinnamoyl-beta-phenethylamine and N-acyldopamine derivatives. *Chem. Pharm. Bull*. 40(2):396-400.

28. Yueh-Hsiung K., Ming-Jai S. (2012) *Catechol-based derivatives for treating or preventing diabetics.* US8088818.

29. Bernardo J., (2004) *Vitamin D analogues.* US6689922.